Climatic mean and interannual variation of northern Barents Sea water mass distribution and circulation

A combined study of ROMS, current and hydrography observations

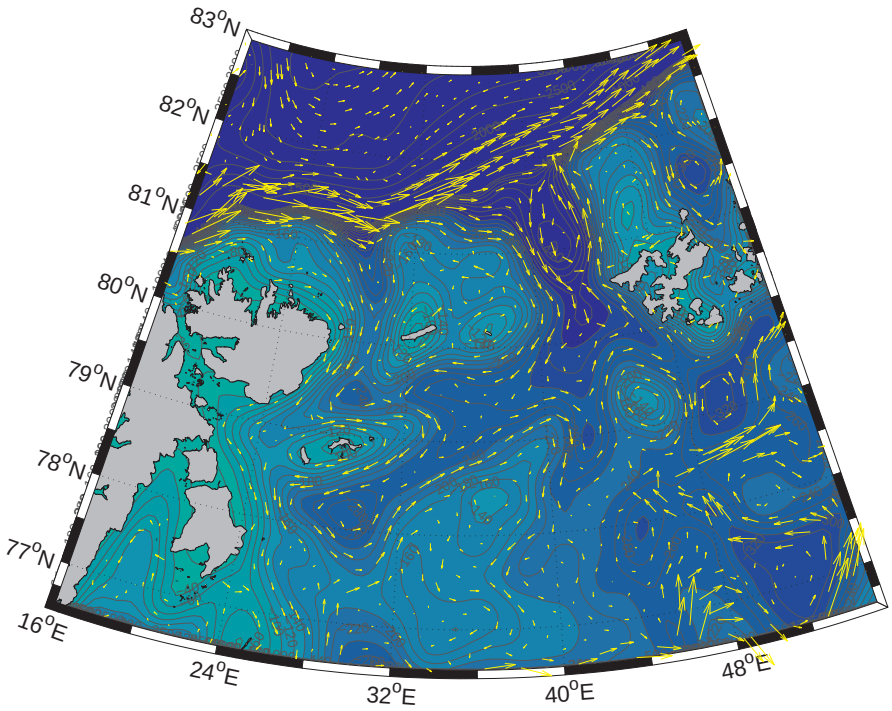

Master thesis in climate
Sigrid Lind Johansen
June 2008

Geophysical Institute
University of Bergen

Abstract

Evaluating current measurements, hydrography observations and model (ROMS) results of the northern Barents Sea, water mass distribution and circulation is investigated. Water mass exchange with the Arctic Ocean is linked with interannual variation of the Svalbard branch. The validity of ROMS in the study region is discussed.

ROMS give typically barotropic and topographically steered currents, flowing in narrow bands approximately 10-50 km wide. Current directions differ highly from previous interpretations of the flow from hydrographical observations, yet they are consistent with current meter observations in the region.

Model validation indicate ROMS water masses are too saline, however the vertical salinity distribution is close to the observed, and that temperatures are too high especially for Surface and Arctic Water. It is evident Atlantic Water in the Svalbard branch descents under Arctic Water too far east in the model, biasing the inflow towards too much Atlantic Water high up in the water column.

Atlantic Water intrudes the region from north as parts of the Svalbard branch follow topography into the troughs of the Northern Barents Sea Opening (NBSO), the Franz Victoria Trough and Kvitøya Strait. Estimates of model transports show the interannual variation of mass transport in the Svalbard branch could explain nearly 50% of the interannual variation of mass inflow through the NBSO with a time lag of one year. The estimates also show interannual variation of heat transport in the Svalbard branch could explain 37% of the interannual variation of heat transport into the northern Barents Sea through the NBSO.

After entering the northern Barents Sea, Atlantic Water follows topography and gradually loosing its heat content primarily from mixing with Arctic Water.

Model results and observations support water mass modifications from brine enrichment during sea ice formation and cooling of Arctic and Surface Water on Storbanken produce Cold Halocline Water. The model gave Cold Bottom Water in its depressions and a bottom-intensified cold current in the Franz Victoria Trough.

These flows add up to a net mass and heat transport of 0.33 Sv and 7.6 TW into the Barents Sea through the NBSO, where the Franz Victoria Trough dominate the heat transport and the Kvitøya Strait dominate the mass transport. The largest contribution to the net heat transport is due to warm water inflow in Franz Victoria Trough.

Preface

Comes the morning
When I can feel
That there's nothing left to be concealed
Moving on a scene surreal

Eddie Vedder - "Into the Wild"

The morning I deliver my thesis is here. It is certainly surreal. I need to thank music for keeping my spirits up whenever the Barents Sea tried to drown me. But more importantly, there are some people who kept me standing and looking forward during this year.

Thank you Tor Gammelsrød - supervisor at the Geophysical Institute - for great inspiration and advices, Randi Ingvaldsen and Lars Asplin - supervisors at the Institute of Marine Research in Bergen - for giving me this interesting assignment and always meeting me with a smile, Vidar Lien - stand-in supervisor at IMR whenever ROMS played hard to get, UNIS and its great people - for giving me the opportunity of exploring the Arctic nature and understanding some of it.

Friends and family, especially Anna Birgitta for colors and meaningful conversations, Eirik for dreams of mountains to climb, Marianne for safety and realistic opinions, and hospitality during the last tough weekend, Maiken and Alva for sharing their home, Eli Anne for the fun of life, Ilona for new perspectives, Marius for the song and Marco for the dance and the spirit.

There are so many to thank I can't mention you all here. Closing this up and now passing my thesis to the world I need to say the greatest thanks is to Mother Nature for her magnificent mysteries.

Contents

List of Figures

List of Tables

Chapter 1

Introduction

The Barents Sea -a shelf sea influencing the Arctic Ocean

The Barents Sea is the deepest shelf sea in the vicinity of the Arctic Ocean with an average depth of 230 m. It is situated north of Norway and limited by Svalbard and Franz Josef Land in the north, by Novaya Zemlya in the east, and by the continental slope in the west, see Figure 1.1. Storbanken is the largest bank, separating the northern Barents Sea water masses from the southern. The shallow regions are especially important in water mass transformations due to sea ice formation and brine release. *Nansen* (1906) proposed water mass transformations in the Barents Sea contribute deep water for the Eurasian Basin, and that the Barents Sea is an important heat sink in the Nordic Seas. *Helland-Hansen and Nansen* (1909) suggested climate variations in the Barents Sea were of an advective nature and stated variations in physical conditions were of great importance for the large biological fluctuations in the Barents Sea. *Loeng* (1991) described the physical oceanographical conditions of the Barents Sea. The current field he presented is still valid in large parts of the Barents Sea.

Observations indicate Barents Sea water mass transformations produce modestly saline water close to freezing point temperature, Cold Halocline Water (CHW) (*Løyning*, 2001). This water mass contribute to maintenance of the cold upper halocline of the Arctic Ocean, separating the cold Arctic Surface Water and sea ice cover from the warmer underlaying water with Atlantic origin (*Aagaard et al.*, 1981). Additionally, winds and tides open polynyas particularly around islands in the Barents Sea, producing high salinity water, Cold Bottom Water (CBW), which may flow down along slopes and fill depressions in the Barents Sea (*Midttun*, 1985). Observed outflow of this water mass show it is dense enough to penetrate down to 500 m depth (*Schauer et al.*, 1997) after leaving the Barents Sea as plumes or bottom-intensified currents in the troughs.

The separation of Atlantic Water in the south from Arctic Water further north is denoted the Polar Front. It is topographically controlled by the slope from Bjørnøya further towards Storbanken and Sentralbanken (*Johannesen and Foster*, 1978; *Harris et al.*, 1998).

The two major freshwater sources to the Barents Sea is sea ice import through the Northern Barents Sea Opening and the Norwegian Coastal Current (*Kwok et al.*, 2005).

Comparable amounts of heat to the Arctic Ocean through Barents Sea and Fram Strait

About half of the heat transported to the Arctic Ocean with the Norwegian Atlantic Current is brought into the Barents Sea between Norway and Bjørnøya, the Barents Sea

Opening (BSO) (*Ingvaldsen et al.*, 2002, 2004; *Skagseth et al.*, 2008). This Atlantic Water (AW) is significantly modified in the Barents Sea from cooling by the atmosphere, mixing with other water masses and salinization from brine release during sea ice formation. The main outflow in the Barents Sea is between Franz Josef Land and Novaya Zemlya, the Barents Sea Exit (BSX). This region is poorly observed; some model studies indicate modified AW flow out here, while other models give mainly cold dense water outflow. Current meter observations 1991-1992 indicate half the net mass transport through BSX to the Arctic Ocean is cold dense water (*Gammelsrød et al.*, 2008). Mass transports through the ∼300 km wide (*Gerdes et al.*, 2003) Northern Barents Sea Opening (NBSO) between Svalbard and Franz Josef Land was estimated one order of magnitude smaller than the other openings of the Barents Sea by *Maslowski et al.* (2004).

It is argued whether the Barents Sea is a heat sink or source for the Arctic Ocean. Significant water mass transformations are known to occur, the question is the total heat budget. *Simonsen and Haugan* (1996) estimated a mean net heat loss of 140 TW from the Barents Sea to the atmosphere. Combining results from several studies, net heat transport into the Barents Sea is approximated 70-80 TW with the contribution from the BSO one order of magnitude larger than the BSX and the NBSO (*Skagseth et al.*, 2008; *Gammelsrød et al.*, 2008; *Maslowski et al.*, 2004; *Gerdes et al.*, 2003).

The other half of the Norwegian Atlantic Current continues northward along the western slope of Svalbard as the West Spitsbergen Current (WSC). Part of the AW in the WSC recirculate in the Fram Strait; mainly the warm core of the current on the upper shelf slope continue into the Arctic Ocean (*Saloranta and Haugan*, 2001). This part of the WSC divide into the Yermak branch and the Svalbard branch at the Yermak Plateau northwest of Svalbard. The latter flow continue eastward along the northern slope of Spitsbergen, Nordaustlandet and the Barents Sea. The Svalbard branch has also been called the Fram Strait Branch by e.g. *Schauer et al.* (1997). The AW in the Svalbard branch has been frequently suggested to dive under the Arctic Surface Water moving in the opposite direction. Other suggestions are gradual cooling and freshening of the upper layer AW. Recent current meter observations by *Ivanov et al.* (2007) indicate the latter process is more likely to occur.

Observations from the northern Barents Sea indicate AW intrudes the region from north (*Pfirman et al.*, 1994; *Løyning*, 2001; *Abrahamsen et al.*, 2006). It has been suggested parts of the Svalbard branch flow into the northern Barents Sea between Victoria Island and Franz Josef Land, the Franz Victoria Trough. Water mass exchange in the NBSO and hydrographic conditions in the northern Barents Sea has been poorly investigated due to its harsh natural environment and extensive sea ice cover.

Modelling the Barents Sea

Numerical ocean models with persistent improved resolution have provided useful indications of the Barents Sea currents and hydrography. Together with observations these simulations improve the knowledge of water mass circulation and modification in the Barents Sea and its exchange with the Arctic Ocean.

Budgell (2005); *Lien et al.* (2006) presented results and validations of the Regional Ocean Model System (ROMS) atmospherically forced with the National Centers for Environmental Prediction (NCEP)/National Center for Atmospheric Research (NCAR) Reanalysis. The BSX water mass exchange was investigated using a ROMS simulation and the Naval Postgraduate School Arctic Modelling Effort (NAME) both atmospherically forced with the European Centre for Medium Range Weather Forecasts (ECMWF) ReAnalysis Project (ERA-40) by *Gammelsrød et al.* (2008).

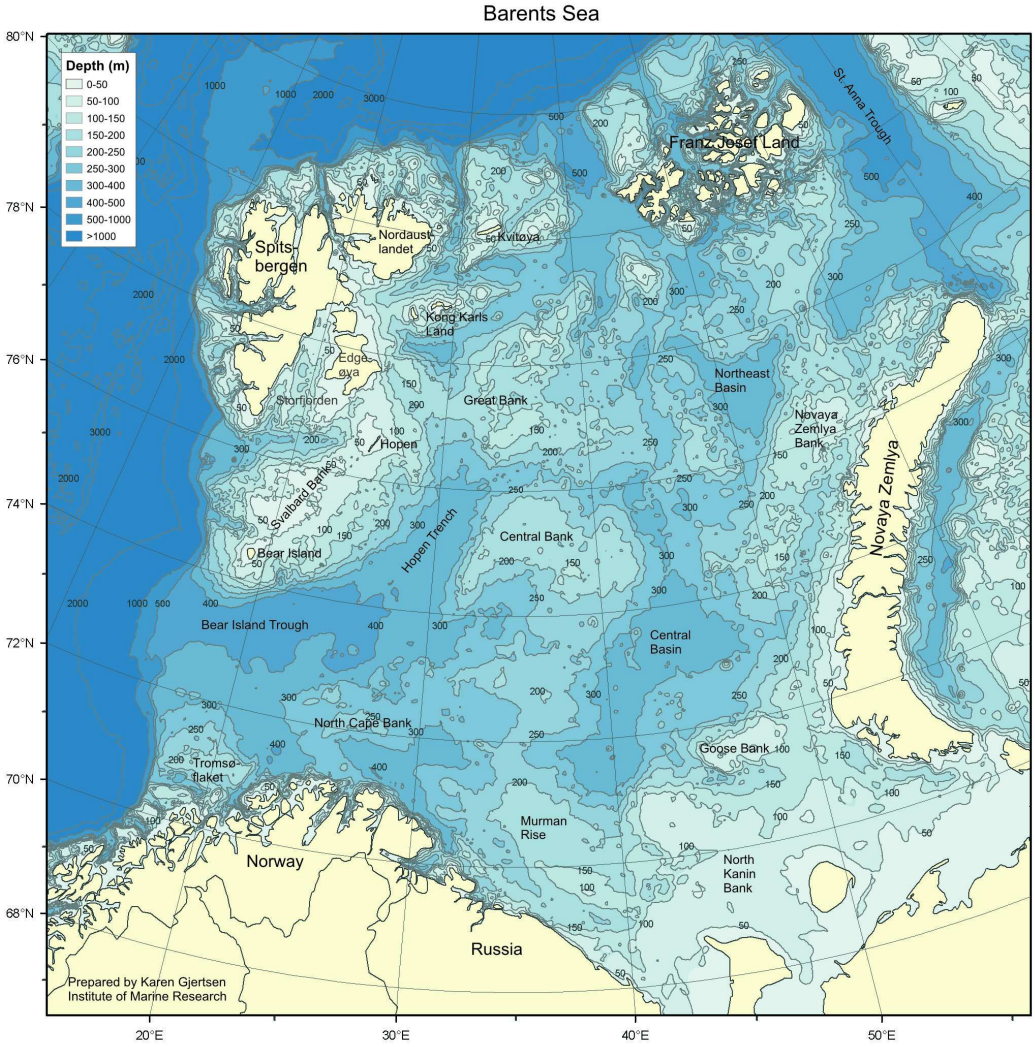

Figure 1.1: Known bathmetry of the Barents Sea. The study region was north of 77°N, from Edgeøya to the Northeast Basin (20-50°E).

Maslowski et al. (2004) published 23-year mean conditions in the Barents Sea and *Kwok et al.* (2005) discussed hydrographical implications of sea ice fluxes to the Barents Sea, both interpreting NAME results with ERA-40 forcing.

Formation of dense water was investigated with the HAMburg Shelf Ocean Model (HAMSOM) using ERA-15 forcing by *Harms* (1997), and with NCEP/NCAR forcing *Harms et al.* (2005) applied HAMSOM in sensitivity studies. Additionally, (*Gerdes and Schauer*, 1997; *Gerdes et al.*, 2003) investigated the role of the Barents Sea for Arctic Ocean water mass distribution and warming events using the Geophysical Fluid Dynamics Laboratory (GFDL) Modular Ocean Model (MOM-2) forced with the NCEP/NCAR Reanalysis.

Key assignments of this thesis

This thesis describe the water mass distribution, transformation and circulation in the northern Barents Sea based on observations from current meters 1980-1983 between Nordaustlandet and Kvitøya, here named the Kvitøya Strait, hydrography data in the northern Barents Sea observed autumns 1981, 1982, 2000 and 2001, and model results from a ROMS hindcast from 1990 through 2001. The model is a coupled three-dimensional baroclinic ice-ocean numerical model atmospherically forced with ERA-40, having a 9 km horizontal resolution and including tides. Model validation for the northern Barents Sea is also performed.

Water mass exchange between the northern Barents Sea and the Arctic Ocean in the region between Svalbard and Franz Josef Land (the NBSO) is investigated and quantified based on the model results.

The AW in the Norwegian Atlantic Current was exceptionally warm in the 1990s due to low heat losses in the Nordic Seas during the positive North Atlantic Oscillation (NAO) phase (*Saloranta and Haugan*, 2001). *Gerdes et al.* (2003) showed velocities in the Svalbard branch were abnormally high in the 1990s, being three times as high in the early 1990s than in the mid-1960s. This indicate the model hindcast presented here (1990-2001) is biased toward warmer than average states of the Barents Sea and possibly larger than average inflow of AW in the NBSO.

Recent observations indicate a warming of the northern Barents Sea (R. Ingvaldsen, personal communication). This may be a signal of adjustments toward a warmer Barents Sea due to global warming, and indicate the region studied here could get increased significance for biological activity in the near future.

Chapter 2

Data and Methods

2.1 Observations

2.1.1 Hydrography observations

The hydrography data was Conductivity Temperature Depth (CTD) profiles from 66 stations observed August 1981 and 57 CTD stations observed August 1982 in the northern Barents Sea, see positions in Figure 2.1. Additionally, 16 CTD stations in the southern Barents Sea from the Vardø-North section observed in August 1981 and August 1982, and totally seven CTD stations north of Kong Karls Land -three of them from September 30 2000 and four September 30 2001, were provided by the Institute of Marine Research. All observations from 1981 and 1982 were part of the data set used by *Pfirman et al.* (1994).

Vertical temperature, salinity and density profiles for all CTD stations were visually investigated. Vertical sections were interpolated from sequential CTD stations for the northern Barents Sea observations August 1981 and 1982. Temperature-salinity profiles from complete data collections and selected stations distinguished water masses and their mixing results. Comparing water mass distribution in CTD sections and stations, and identifying core characteristics from temperature-salinity diagrams, observed northern Barents Sea water mass distribution and circulation was interpreted.

2.1.2 Current meter east of Kvitøya 1980-1983

Figure 2.1 show the position of a current meter mooring observing direction, speed, temperature and salinity from August 1980 to August 1983 in the strait between Nordaustlandet and Kvitøya, the Kvitøya Strait. The rig was changed each year in August and consisted of two Aanderaa RCM-4 recording current meters with a mechanical rotor and vane, temperature and conductivity sensor. The lower instrument was situated 5 m above

Table 2.1: Information about the current meter moorings. Periods of measuring, instrument number, position vertically and horizontally, and total depth.

Measuring period	Instrument	Depth	Total depth	Position
Jul30 80 - Aug25 81	RCM-4 S04887	75 m	260 m	E29°59.0′ N80°01.0′
Jul30 80 - Aug25 81	RCM-4 S04888	255 m	260 m	E29°59.0′ N80°01.0′
Aug25 81 - Aug29 82	RCM-4 S03151	115 m	300 m	E29°58.0′ N80°01.0′
Aug25 81 - Aug29 82	RCM-4 S03163	295 m	300 m	E29°58.0′ N80°01.0′
Aug10 82 - Jul19 83	RCM-4 S06200	105 m	290 m	E29°54.0′ N80°03.0′
Aug10 82 - Aug8 83	RCM-4 S06498	285 m	290 m	E29°54.0′ N80°03.0′

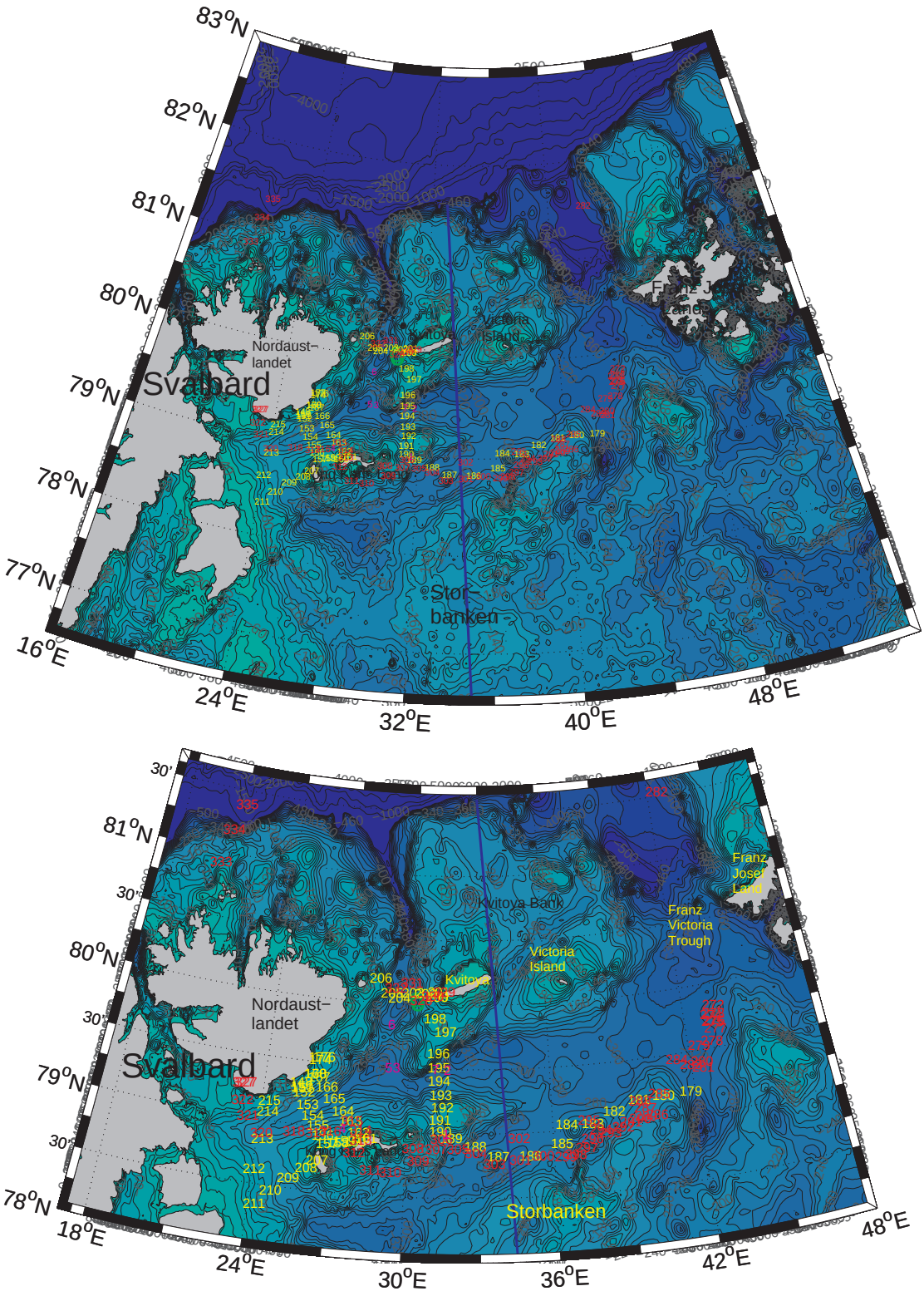

Figure 2.1: Northern Barents Sea bathymetry and position of CTD stations August 1981 (yellow station numbers), August 1982 (red station numbers), a CTD section published by *Løyning* (2001) 1996 (blue line), CTD stations September 30 2000 and 2001 (purple station numbers), and current meter observations west of Kvitøya 1980-1983 (green circles). Bathymetry from the National Geophysical Data Center ETOPO2 database.

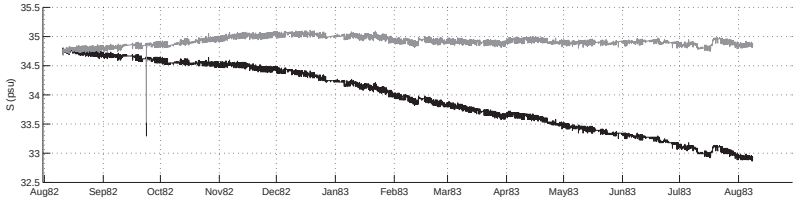

Figure 2.2: Salinity time series at lower current meter at 285 m depth from August 1982 to August 1983. Original salinity in black line. Corrected salinity in grey line was found by $S(t) = S_0(t) + k \cdot t$, where $S(t)$ is the corrected salinity at time t, $S_0(t)$ is the original salinity at time t, $k = 0.00022364$psu/hour is the salinity drift found by linear regression of original salinity, and t is the number of hours since the first measurement (measurements were made ones per hour).

the sea bed in a warm core and the upper from 75 to 115 m depth in a cold core, see Table 2.1. One hour averaged speed and direction, and point measurements each hour of temperature and conductivity was observed. The measurements from August 1980 to August 1981 were published by *Aagaard et al.* (1983).

Errors were seen in the measurements at the lower meter each year. Deterioration of the speed caused by growing sea weed on the mechanical rotor occurred from April to August 1981, throughout the whole year 1981-82 and from March to August 1983. Additionally, the conductivity sensor drifted toward lower values all three years and a false electronic signal appeared repeatedly in the temperature sensor in 1981-82. Assuming a constant drift of each sensor each year, the salinity was corrected by linear regression and due compensation of the salinity, see Figure 2.2.

After correcting the salinity drift CTD profiles near the current meters were compared with the current meter observed temperature and salinity. This comparison showed the salinity of the upper meter 1980-81 was about 1 psu too high, supported by the one-year mean salinity of the upper meter being 1.3 psu higher than the lower meter. Hence, a constant value of 1 psu was subtracted from the salinity observations at the upper meter 1980-81. The other time series of temperature and salinity were comparable to the CTD observations.

Figure 2.3 show the tides in the current meter measurements were smoothed out applying the PL64 filter described by *Rosenfeld* (1983). The filter had a half amplitude period of 33 hours and a half power period of 38 hours, and the time series were folded over and cosine tapered at each end to return a filtered time series of the same length as the original data.

2.2 Ocean model

2.2.1 Model description

Results from the Regional Ocean Modelling System (ROMS) version 2.1 simulation of the Barents Sea were provided by the Institute of Marine Research for the time period January 1 1990 to December 31 2001.

Budgell (2005) described the model setup. It coupled a dynamic-thermodynamic sea ice model with a three-dimensional baroclinic ocean general circulation model. The dynamics of the sea ice module were based on elastic-viscous-plastic rheology, the thermodynamics consisted of two ice layers and one snow layer to solve the heat conductivity equation. A molecular sub-layer between the sea ice bottom and the ocean was included, giving more realistic melting and freezing rates.

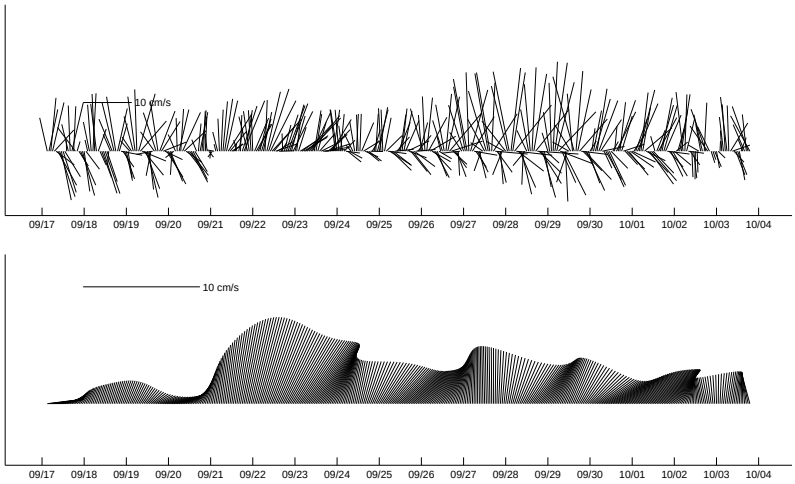

Figure 2.3: Stickplot of selected period showing how the tides are smoothed out applying the PL64 filter described by *Rosenfeld* (1983). Original current observations with measurement every hour at upper current meter September 17 1982 - October 3 1982 (upper figure), and filtered time series of the same period (lower figure). Scaling of arrows indicate the filtered data had smaller velocities than the original.

The ocean module had a large area model supplying initial and boundary conditions to the regional Barents Sea model. The large area model had a stretched spherical sinusoidal horizontal grid, allowing 50 km resolution in the Barents Sea. In the vertical 30 generalized topography following s levels, stretched to enhance resolution close to surface and bottom boundaries, were applied. The time step was 1800 s (30 min); atmospheric forcing was the NCEP/NCAR Reanalysis. Tides were not included in the large area model. It started from rest January 1 1948 and spinned up to the end of 1987. January 1 1988 was then used as initial conditions for a hindcast from January 1 1948 to the end of 2003.

The regional Barents Sea ocean model used the same horizontal and vertical coordinate system as the large area model, with a higher horizontal resolution (7.8 to 10.5 km; average 9.3 km) and a time step of 450 s (7.5 min). A Generic Length Scale (GLS) k-kl local turbulence closure scheme was used in order to produce good resolution in coastal regions where tidal mixing is important. The boundaries of the regional model were forced by interpolated 5-day mean fields from the large area model, and tidal velocities and free surface heights from eight constituents of the Arctic Ocean Tidal Inverse Model (AOTIM). Atmospheric forcing of the regional model was ERA-40 -the main difference from the simulation described by *Budgell* (2005). Initial conditions were 5-day mean large-area model fields interpolated for January 1 1990. The simulation of the regional model was performed from 1990 to 2002.

Daily averaged velocity, temperature and salinity fields from the model results were interpolated on a horizontal grid with 9 km resolution in 14 z levels: 0, 10, 20, 30, 40, 50, 75, 100, 125, 150, 200, 250, 300 and 400 m depth. These interpolated fields were used in this thesis. Tides could not be read out of the results even though they were included in the regional model since the fields were given as daily averages.

Figure 2.4 shows the bathymetry of ROMS was smoother than the real, resulting in shallower straits and deeper banks compared with the actual sea bed seen in Figure 2.1. Thus regions of islands close to straits, such as Kvitøya, Victoria Island and Franz Josef Land appeared as banks with up to 120 m of water above them in ROMS.

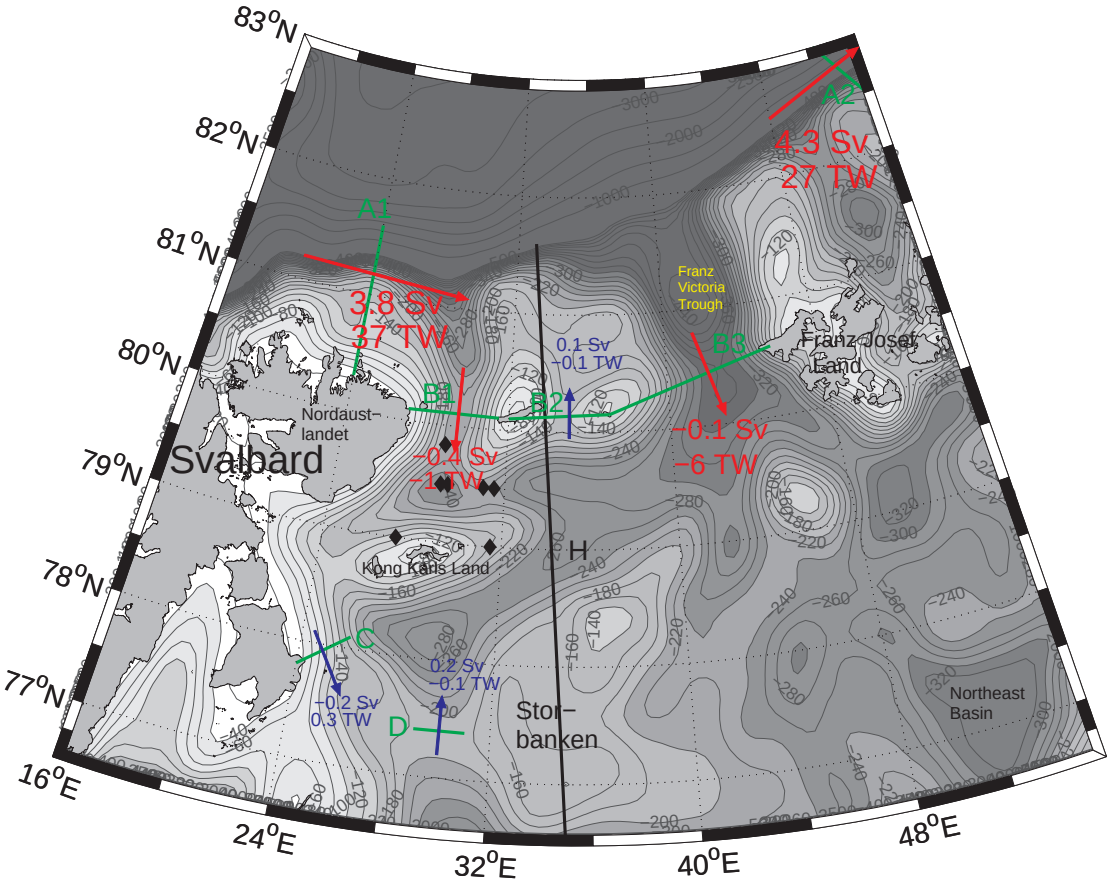

Figure 2.4: ROMS bathymetry, transport sections (green lines; marked A1-D), hydrography section August 1 1996 (black line; marked H), and grid points for vertical hydrography profiles north of Kong Karls Land (black diamonds). Model 12-year mean net mass and heat transport is indicated for each section. Additionally, temperature and velocity was extracted for a vertical section along 80.1°N from Svalbard to Franz Josef Land.

2.2.2 Analyzing the model results

12-year and one-year mean velocity, temperature and salinity fields were produced from the daily averaged fields each depth. An overview of the mean, spatial and temporal variation was achieved by visually comparing the mean fields for the 14 depths. Considering the bathymetry of ROMS and model hydrography and currents, time series of volume, heat and salt transport in seven sections crossing the assumed most essential flows, were extracted from the model results, see Figure 2.4.

This provided 12-year time series of daily averaged spatial sum of positive, negative and net transport across each section. 12-year mean values and standard deviations of daily average transports were produced. In order to investigate interannual transport variations, the time series were filtered with a 365-days running mean applying a symmetric Hanning window. The first and last 182 days of the filtered time series were badly represented and hence excluded. Applying a lower estimate of 10 degrees of freedom in the filtered and edge-cut time series, correlation coefficients were estimated. The significance level of the correlation coefficients are on a 5% level unless otherwise is mentioned. The square of the correlation coefficients were used as an estimate of how much of the interannual variation could be explained by each correlation.

Daily average temperature and north-south velocity was extracted from the model results in a vertical west-east going section from Svalbard to Franz Josef Land at 80.1°N. 12-year and yearly mean fields of this section provided climatic mean and interannual variation of water mass exchange between the Arctic Ocean and the northern Barents Sea.

2.2.3 Model validation

The observed hydrography in 2000 and 2001 was compared with modelled temperature and salinity. Vertical profiles at four neighboring grid points (making a square) at the position of each observation were extracted from the modelled temperature and salinity fields. The profiles were made for September 30, the same day as the measurements, and for February 15, August 15, September 15 and October 15 2000 and 2001 in order to reveal significant temporal or spatial shifts in the model, and achieve some indications of seasonal variation in the profiles. Additionally, profiles in other regions of the northern Barents Sea were extracted for September 30 2000 and 2001 enabling comparisons of grid points with large horizontal distance.

The section published by *Løyning* (2001) was compared with a corresponding model section. The appropriate model section was determined by looking at sections along 34, 35 and 36°E every seventh day during July and August 1996. Minor spatial and temporal variations were seen, 35°E August 1 1996 was the regarded the most representative section and hence chosen for the comparison.

Chapter 3

Results

3.1 Observed hydrography in the northern Barents Sea

The water masses in the northern Barents Sea defined from all hydrography observations presented here are seen in Table 3.1.

3.1.1 August 1981 and 1982

Positions of CTD stations observed late August 1981 and 1982 are shown in Figure 2.1. Figure 3.1 and 3.2 shows the most representative vertical temperature and salinity sections of these observations. Vertical density sections had almost identical structure as the corresponding salinity sections (not shown).

The Surface Water (SW) had temperatures from -1.5 to 2°C and salinity 32 to 34 psu. It was separated by a sharp halocline at around 20 m depth from Arctic Water (ArW) colder than 0°C and salinity 34 to 34.5 psu. The most saline ArW with a maximum of 34.7 psu was observed above the northeastern part of Storbanken both years.

Below the ArW, Atlantic Water (AW) was generally observed with temperatures from 0 to 1.3°C and salinity around 34.7 psu. The AW core was situated at 250 m depth in 1981 and 200 m depth in 1982, and its maximum temperature of 1.8°C was observed northeast of Storbanken in 1982.

Figure 3.1 (upper) show temperature and salinity sections August 1981 between the island Storøya near the northeast end of Nordaustlandet and Kvitøya, crossing the Kvitøya Strait. The figure shows cores of ArW and AW on the eastern side of the strait. A similar structure was observed August 1982 (not shown).

Temperature and salinity sections from Kvitøya southwards to Kong Karls Land are seen in Figure 3.1 (middle). At Station 194 it is seen a patch of AW close to the sea bed and an ArW core above. The AW here was colder and less saline than that observed in the Kvitøya Strait. The position of this station in Figure 2.1 shows this is in the narrow

Table 3.1: Water mass characteristics.

Water mass	Depth (m)	Temperature (°C)	Salinity (psu)
Surface Water (SW)	0-20	-1.5 to 2	32-34
Arctic Water (ArW)	40-150	-1.8 to 0	34-34.7
Cold Halocline Water (CHW)	70-80	< -0.5	34-34.5
Atlantic Water (AW)	150-300	0 to 2.2	34.75-34.9
Cold Bottom Water (CBW)	200-350	-1.9 to 0	>34.75

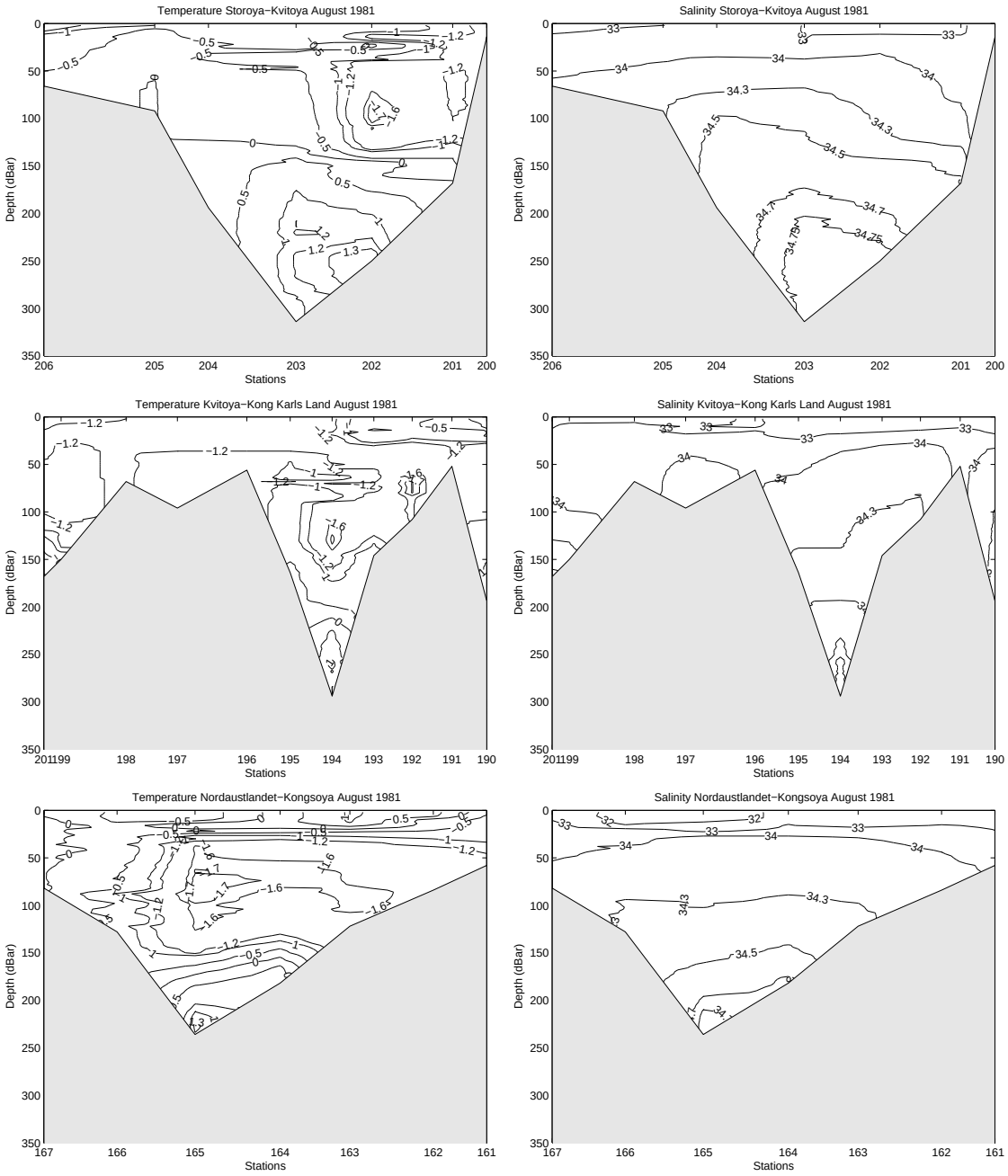

Figure 3.1: Observed temperature (left figures) and salinity (right figures) between Storøya and Kvitøya August 1981 (upper), between Kvitøya and Kong Karls Land August 1981 (middle), and from Nordaustlandet to Kongsøya August 1981 (lower).

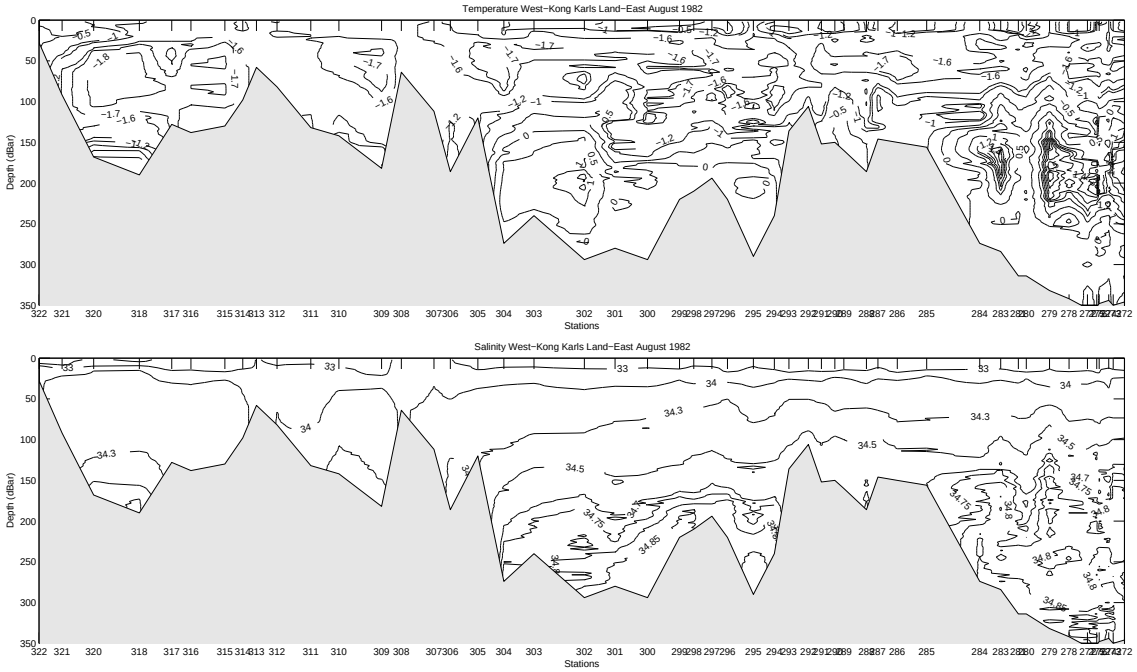

Figure 3.2: Observed temperature (upper) and salinity (lower) from Nordaustlandet to Kong Karls Land and further east passing Storbanken August 1982. Positions of stations seen on map in Figure 2.1.

connection between the southern extension of the Kvitøya Strait and the main deep region in the northern Barents Sea.

Figure 3.1 (lower) show the section from Nordaustlandet to Kongsøya, the largest island of Kong Karls Land. AW was also here observed close to bottom at the deepest station, with similar properties as in the Kvitøya Strait. The figure furthermore shows a wider and colder ArW core than the previous shown sections. At the coast of Nordaustlandet water slightly warmer and fresher than the surroundings was observed. This was also seen in the two other sections from Nordaustlandet and southeastwards (not shown; positions of sections seen in Figure 2.1). These sections also showed the AW core got colder towards south. In the section from Kong Karls Land and southwestwards, AW was not observed at all (not shown).

Figure 3.2 shows the west-east going section crossing almost the whole northern Barents Sea along approximately 79°N in 1982. Figure 2.1 showss it starts at Nordaustlandet, crosses Kong Karls Land and continues along the northwestern slope of Storbanken to the deep region northeast of Storbanken. The section shows the deep region north of Storbanken had the warmest and most saline AW core, reaching 1.8°C and 34.8 psu. The deep region between Kong Karls Land and Storbanken had slightly fresher and colder AW with maximum temperature 1.3°C. The region between Nordaustlandet and Kong Karls Land was mainly occupied by very cold ArW with salinity less than 34.3 psu. The AW core at the bottom here was even colder and fresher being 1°C and 34.7 psu. Additionally, Figure 3.2 showss the deepest 100 m east and west of Storbanken were occupied by high salinity water (S>34.8 psu) with temperature about 0°C.

A section going from the northeast edge of Storbanken to Kong Karls Land observed August 1981 (not shown) had quite similar vertical distribution as Figure 3.2.

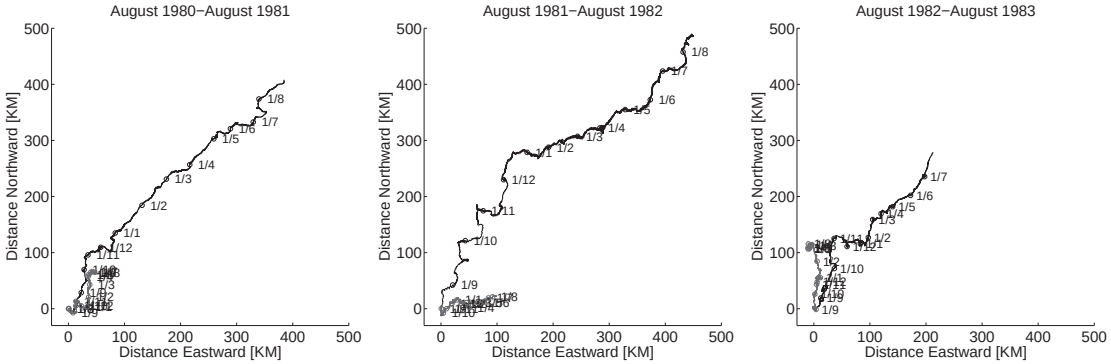

Figure 3.3: Progressive vector of measured currents 1980-81 (left), 1981-82 (middle), and 1982-83 (right). Black line denotes upper meter; gray line lower. The circles denote the first day of a month (see dates).

Table 3.2: Statistics of measured (unfiltered) speed (cm/s), eastern velocity component U (cm/s), northern velocity component V (cm/s), temperature T (°C) and salinity S (psu) for each year of current meter measurements west of Kvitøya. Yearly mean values in upper row and standard deviations in lower row each current meter.

Current meter		Velocity			Temperature	Salinity
Depth	Year	Speed	U	V		
75 m	1980-81	7.1	1.1	1.2	−1.0	34.5
		3.6	3.2	7.1	0.6	0.5
255 m	1980-81	3.5	0.1	0.2	1.0	34.7
		1.6	2.3	3.1	0.3	0.1
115 m	1981-82	11.7	1.4	1.5	−0.3	34.4
		6.4	4.9	12.2	0.8	0.1
295 m	1981-82	3.6	0.3	0.1	1.0	34.4
		2.8	2.2	4.0	0.7	0.6
105 m	1982-83	7.0	0.7	0.9	−0.2	34.2
		3.3	3.2	7.0	0.8	0.1
285 m	1982-83	3.8	−0.03	0.4	1.6	34.9
		1.8	2.4	3.4	0.3	0.1

3.1.2 CTD September 2000 and 2001

Vertical profiles of the CTD stations north of Kong Karls Land September 2000 and 2001 are shown in Figure 4.1. The figure shows the SW was much colder and fresher in 2000 than 2001. The core of ArW in 2000 and 2001 was slightly warmer than in 1981 and 1982, and completely absent in two stations in 2001, where the upper 100 m were still summer heated. AW reached 1.3°C and 34.8 psu in 2000. AW was warmer and occupied a larger part of the water column in 2001, reaching 2.2°C.

3.2 Measured currents west of Kvitøya 1980-1983

The progressive vector in Figure 3.3 shows northeastern currents dominated at the upper meter (75-115 m depth) 1980-1983, while currents at the lower meter (255-295 m depth) varied from northern to eastern and were one order of magnitude smaller than the upper. Temporary incidents of a southern component occurred at the lower meter some months, mainly in autumn.

Table 3.2 summarize mean values and standard deviations for each current meter.

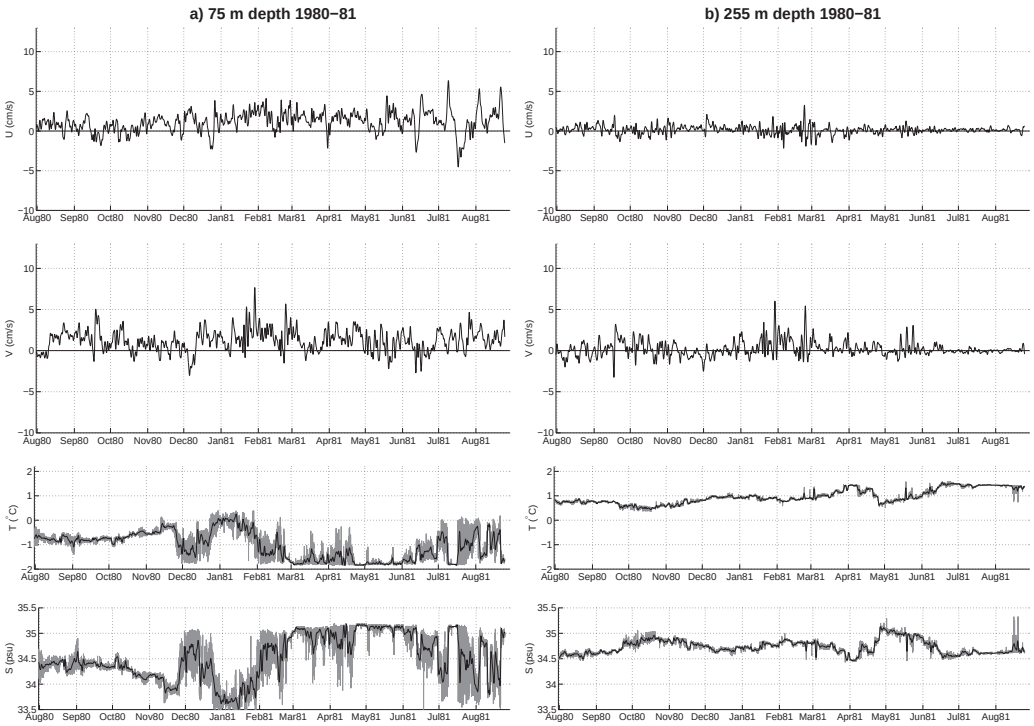

Figure 3.4: Filtered eastern velocity component U, filtered northern velocity component V, original (grey line) and filtered (black line) temperature T and salinity S. Observed at 75 m depth a) and 255 m depth b) from July 30 1980 to August 25 1981. At 255 m depth, U and V had errors after March 1981, and salinity is corrected as described in Figure 2.2.

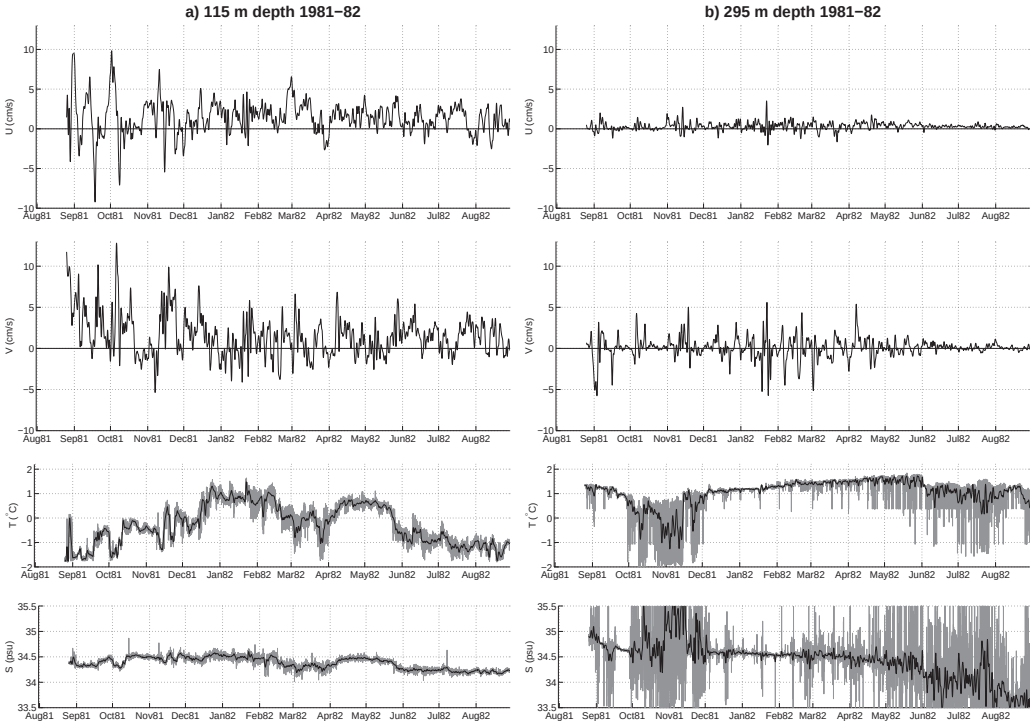

Figure 3.5: Same as Figure 3.4 with observations at 115 m depth a) and 295 m depth b) from August 25 1981 to August 29 1982. The observations at 295 m depth had errors in all parameters.

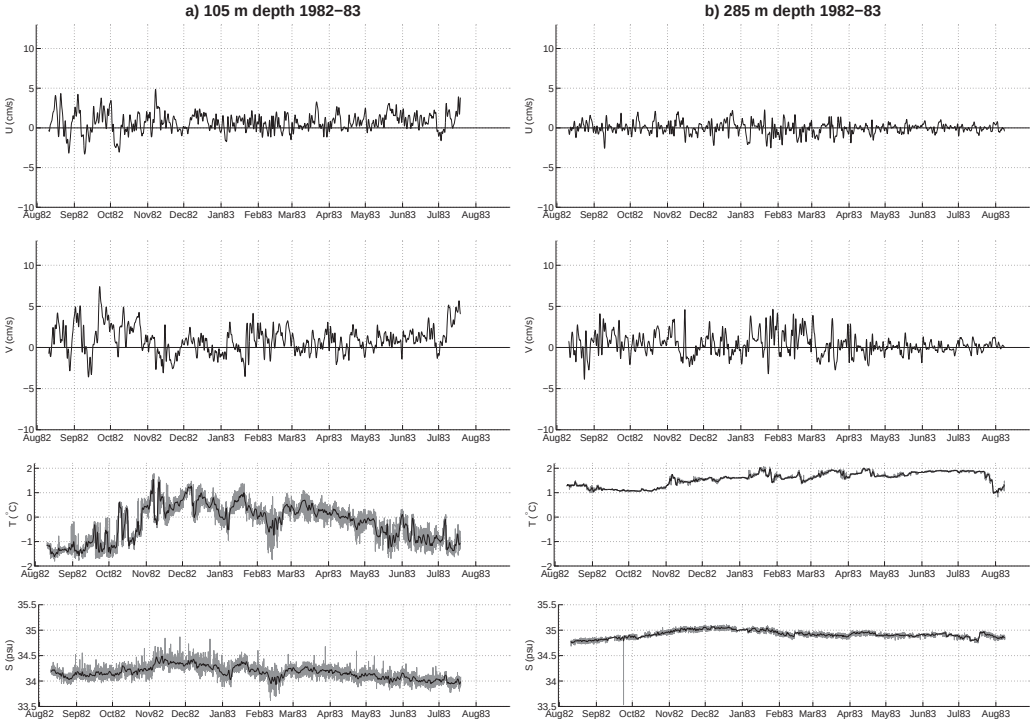

Figure 3.6: Same as Figure 3.4 with observations at 105 m depth from August 10 1982 to July 19 1983 a), and 285 m depth from August 10 1982 to August 8 1983 b). At 285 m depth, U and V had errors after April 1983, and salinity is corrected as described in FigureSalCorr.

A much larger speed than eastern (U) and northern (V) velocity components is easily recognized. This is due to tidal motion in the strait.

Figures 3.4-3.6 shows the filtered time series of U and V (tides smoothed out), and original and filtered time series of temperature and salinity.

Figure 3.4 a) show the upper meter 1980-81 measured cold temperatures. In August and September it was around $-0.7°$C, and then increased steadily to $0°$C in November. At the end of November temperatures dropped rapidly and fluctuated more, reaching $-1.8°$C occasionally. It increased quickly to $0.3°$C in January and dropped again in February, being $-1.8°$C with short incidents of slightly warmer water until June. The summer months showed large temperature variations and a warming trend.

Figure 3.4 a) also show the salinity at the upper meter had a large variation from 33.5 to 35.2 psu. It typically increased when temperatures dropped, and periods with $-1.8°$C often coincided with salinity 35.2 psu. Figure 3.4 a) also show the currents at the upper meter 1980-81 were slightly stronger during winter. The eastern velocity component had a larger variation in summer, and during a week in mid-July, a 5 cm/s westward current coincided with $-1.8°$C and 35.2 psu.

Figure 3.4 b) show the lower meter 1980-81 had less variation in temperature and salinity than the upper meter. The figure also shows this meter was in a warmer and more saline water mass than the upper meter, with around $1°$C and 34.7 psu. The filtered velocity components at the lower meter was smaller than the upper, except during January and February 1981 when it was comparable to the upper meters velocity.

Figure 3.5 a) show the upper meter 1981-82 had larger variations and higher temperatures and velocities than the upper meter 1980-81. A pronounced temperature increase was observed in winter with maximum $1.5°$C, and there was very few incidents of $-1.8°$C.

This meter had the strongest current observations and very high variation in autumn. It was situated deeper than the upper meter 1980-81. Additionally, the salinity was very stable compared with the upper meter 1980-81.

The lower meter 1981-82, seen in Figure 3.5 b), had large errors in all parameters throughout the year. The results are presented since the large temperature variations from 1 to -1.8°C in October and November 1981, and from 1.5 to -1.5°C during summer 1982, could be realistic. Overall it measured higher temperatures than the upper meter the same year, and was also slightly warmer than the lower meter 1980-81.

Figure 3.6 a) show the upper meter 1982-83 had very similar temperatures as the upper meter 1981-82. Also the salinity observations were quite similar to upper meter 1981-82, however slightly fresher. The velocity variation was less than for the upper meter 1981-82, however increased in autumn like the previous year.

Figure 3.6 b) show the lower meter 1982-83 had very similar observations as the lower meter 1980-81, however slightly warmer and more saline.

3.3 ROMS simulated water mass distribution, circulation and transports

Climatic mean of model temperature, salinity and velocity fields in the northern Barents Sea for the period January 1 1990 to December 31 2001 are presented below. Additionally, climatic mean and interannual variation of water mass exchange in the Northern Barents Sea Opening (NBSO) is shown.

3.3.1 Climatology

Hydrography fields

Figure 3.7 shows 12-year mean model temperature and salinity fields at surface, 50 and 200 m depth. The figure shows model SW was -0.5 to 1°C, colder above Storbanken and toward east, with salinity around 34.5 psu increasing southwards. From 50 m and deeper, the model gave salinity 34.8 psu or more in the whole northern Barents Sea.

According to definitions of water masses from observations in Table 3.1, the model had ArW only from surface to 30 m depth. However, investigations in Chapter 4.1.2 indicate the model had generally too high salinity. Hence water colder than 0°C and salinity from 34.5 to 34.9 psu was recognized as ArW in the model results. Applying this definition, model ArW concentrated above Storbanken and eastwards from surface to 150 m depth.

Figure 3.7 also show the model gave AW north of Nordaustlandet stretching eastwards and increased temperature with depth, the 2°C isotherm reaching 40°E at 50 m depth. AW core temperature was 2.5°C and the salinity reached 35 psu. The AW extends southwards into the Kvitøya Strait and the Franz Victoria Trough, where it continues westward south of the Kvitøya Bank. Additionally, the model gave AW in the northern edge of the Hopen Trench (30-32°E, 77°N).

Three depressions east of Storbanken were colder than -1.5°C and had salinity 34.95 to 35.05 psu from 125 m and deeper, with minimum temperature -1.7°C occurring at the northernmost depression.

The model gave a strong horizontal salinity and temperature gradient at 81°N at all depths, resembling the front between ArW in the Arctic Ocean and AW in the Svalbard branch flowing eastwards along the northern slope of the Barents Sea.

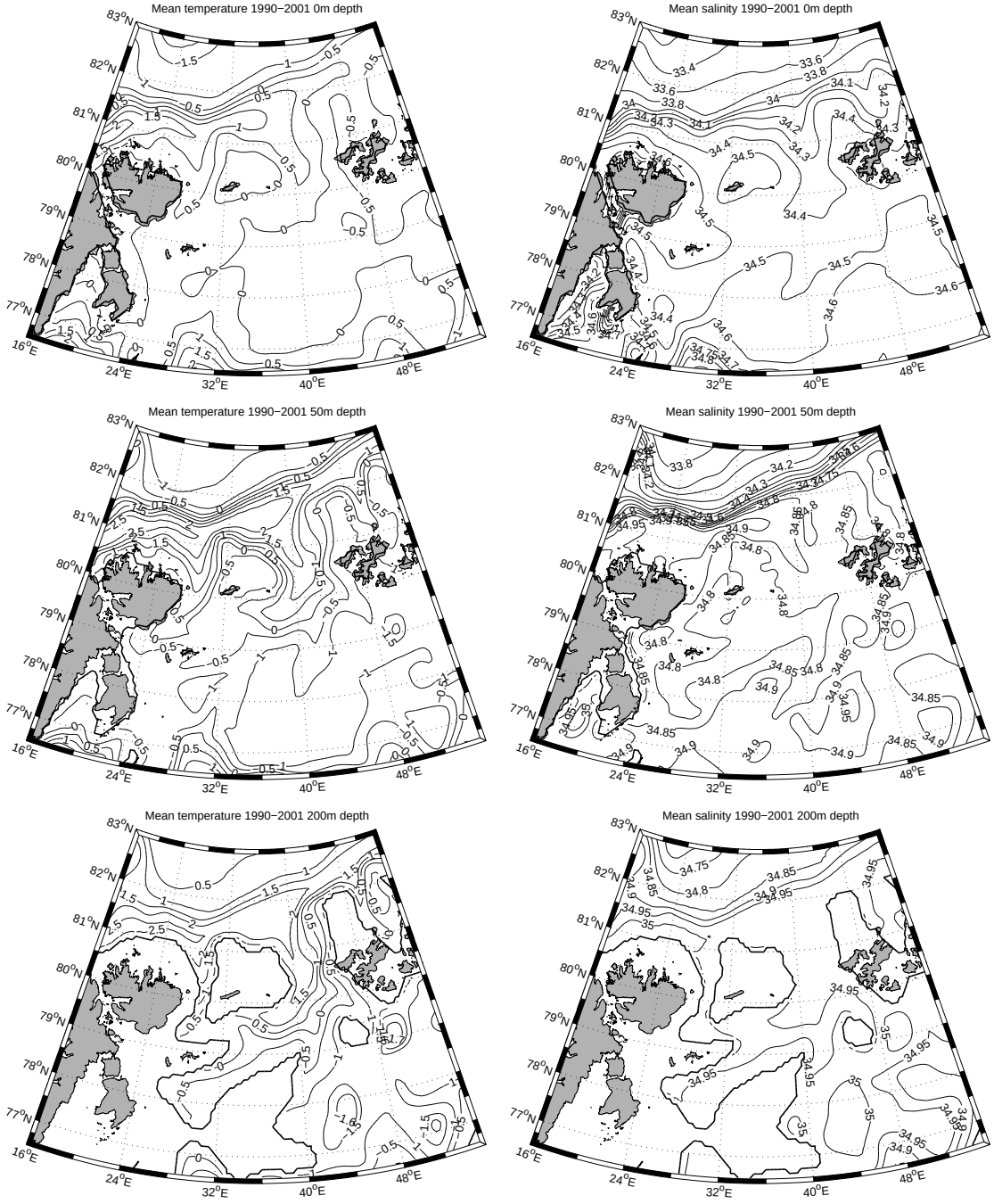

Figure 3.7: 12-year mean temperature (left figures) and salinity (right figures) at surface (upper), 50 (middle) and 200 m depth (lower) of ROMS.

Velocity fields

Figure 3.8 a) show the 12-year mean model velocity field at 50 m depth with ROMS bathymetry. The figure shows currents followed the bathymetry closely. Velocity fields at other depths were highly similar (not shown). Figures 3.8 b) and c) show 12-year mean model velocity fields with speed (colorbar) at 50 and 150 m depth respectively. It is seen the model typically had barotropic currents in narrow bands (10-50 km wide) and speed 4 to 8 cm/s.

The Svalbard branch had maximum speed 25 cm/s and increased somewhat in speed with depth. An extension of this current in the Franz Victoria Trough followed the 300 to 340 m depth contour, and increased slightly in strength below 125 m depth. Some recirculation occurred in the Franz Victoria Trough mainly at upper levels. West of Franz Josef Land a current followed the slope northwards. The Svalbard branch also had an extension through the Kvitøya Strait following the 200 m depth contour.

Figure 3.7 shows the two extensions of the Svalbard branch in Franz Victoria Trough and Kvitøya Strait transported AW into the Barents Sea from approximately 50 m and deeper. Figure 3.8 a) show both continued in an anticyclonic circulation pattern from north of Kong Karls Land to south of these islands, proceeding in a cyclonic circulation in the deep region south of Kong Karls Land, Olga Basin, and then followed the 230 m depth bathymetry contour northeastwards at the northwestern edge of Storbanken.

Figure 3.8 a) also shows the model East Spitsbergen Current follow the east coast of Nordaustlandet towards the Hinlopen Strait, continuing southeastwards along Barents and Edge Islands and southwards east of Hopen Island. This distinct current follows the 60 to 80 m depth contour and was centered around 50 m depth.

Additionally, the 12-year mean current field on Storbanken had two anticyclonic circulation cells. Also, the small bank situated at 48°E 79°N southwest of Franz Josef Land had a distinct anticyclonic gyre around it.

Figure 3.8 a) also show a current following the 240-300 m depth contour from the southern Barents Sea, twisting and turning around the depressions and elevations east of Storbanken, ending up south of Franz Josef Land and continuing eastwards to the Barents Sea Exit (BSX). Figure 3.8 b) and c) show it was strong having speeds up to 20 cm/s, and Figure 3.7 shows this current had temperatures from -0.5 to 0.5°C.

Vertical section from Svalbard to Franz Josef Land

Figure 3.9 shows the 12-year mean temperature (colormap) and northern velocity component (contour lines) in a west-east vertical section from Svalbard to Franz Josef Land at 80.1°N. Note model bathymetry is smoothed, making Kvitøya, Victoria Island and Franz Josef Land appearing as banks instead of islands in ROMS. However, the main water mass motion is circulation on the banks and to a very little degree water mass flow across them, thereby this artifact may not influence the water mass exchange significantly.

The figure shows the model gave predominantly barotropic conditions, and both Franz Victoria Trough and Kvitøya Strait had a warm southward flow on the west side and a cold northward flow on the east side.

The Franz Victoria Trough had the warmest and coldest water masses. Here, AW warmer than 1.5°C and ArW colder than -1°C flowed with 2-4 cm/s southwards and northwards, respectively. The area occupied by currents faster than 4 cm/s was larger on the warm side compared with the cold side. On the east side a bottom-intensified cold current was seen, reaching 6 cm/s.

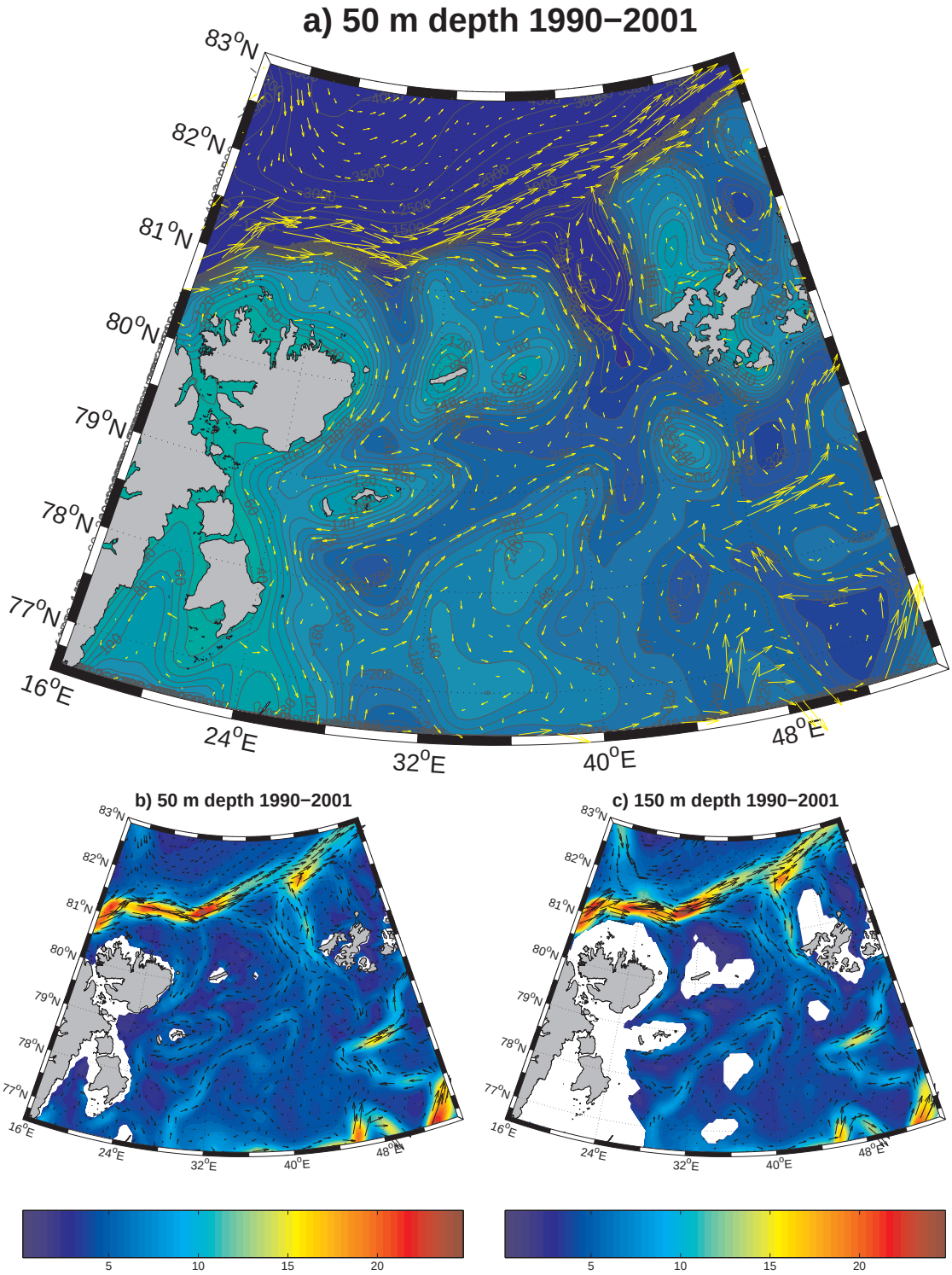

Figure 3.8: Model 12-year mean currents at 50 m depth (yellow arrows) and bathymetry a), at 50 m depth (black arrows) and corresponding speed (cm/s in colorbar) b), and at 150 m depth (black arrows) and corresponding speed (cm/s in colorbar) c). Speed plotted at every eight grid point with arrows doubled in size.

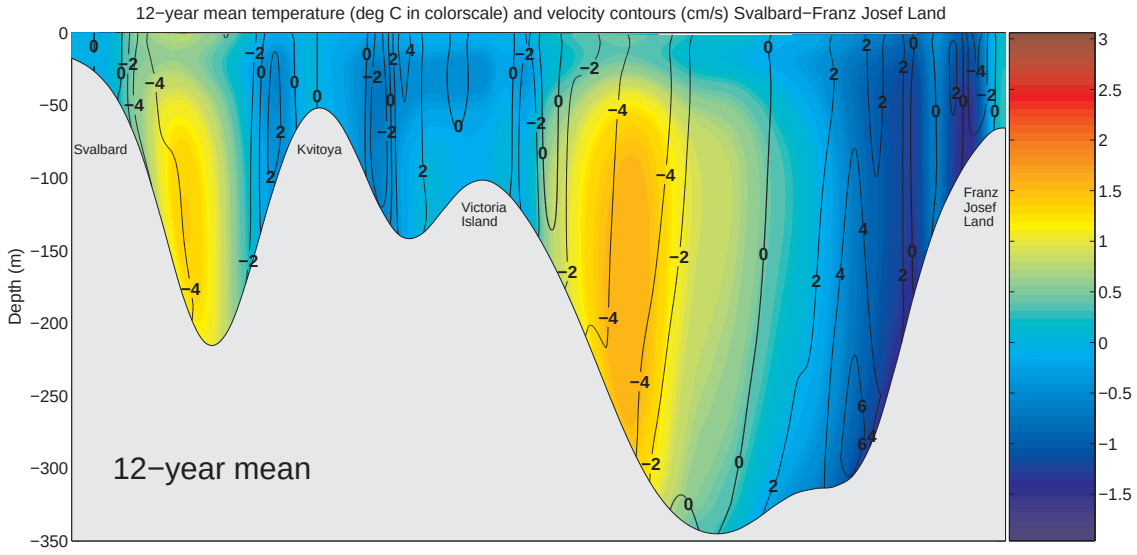

Figure 3.9: Model 12-year mean temperature (colorbar) and north-south velocity (contour lines) in a west-east vertical section between Svalbard and Franz Josef Land at 80.1°N. Positive velocities are northward and negative southward.

Figure 3.9 also show the warm southward current in the Kvitøya Strait between Svalbard and Kvitøya reached 4 cm/s, hugging the steep slope on the western side. The cold northward current was slower and more narrow.

Mean transports

Mass, heat and salt transports in the sections shown in Figure 2.4 were extracted from the ROMS simulation. 12-year mean values and standard deviations of these transports are listed in Table 3.3. Positive direction was defined northward in a east-west oriented section, and eastward in a north-south oriented section.

Daily average heat transport Q through a given section was calculated

$$Q = c_w \sum_{i=1}^{n} \sum_{j=1}^{m} A_{i,j}\, \rho_{i,j}\, v_{i,j}\, (T_{i,j} - T_{ref}) \tag{3.1}$$

where $c_w = 4000\text{Jkg}^{-1}\text{K}^{-1}$ is the specific heat of sea water, $A_{i,j}$ is the area covered by the grid point (i,j), $\rho_{i,j}$ is the sea water density, $v_{i,j}$ is the velocity normal to the section and $T_{i,j}$ is the temperature of the grid point (i,j) this day, and $T_{ref} = -0.1°\text{C}$ is the reference temperature. Water colder than T_{ref} is referred to as cold water and warm water is warmer than T_{ref}. This means heat northward is positive and heat southward negative; cold water northward counts negative while cold water southward counts positive. Reference salinity was 0.0 psu.

Sections A1 and A2 crossed the Svalbard branch before and after its water mass exchange with the northern Barents Sea in the NBSO. It had the largest net mass and heat transport with 4 Sv and 37 TW in Section A1 from Nordaustlandet and northward, and 4 Sv and 27 TW in Section A2 north of Franz Josef Land. The net salt transport increased from 132 to $150{\cdot}10^3\text{kgs}^{-1}$ from Section A1 to A2.

Section B from Svalbard to Franz Josef Land covered the Northern Barents Sea Opening (NBSO) and consisted of Sections B1, B2 and B3. The model gave the largest transports in the NBSO in the Franz Victoria Trough (Section B3), where both mean northward

Table 3.3: 12-year mass, heat and salt transports for the sections seen in Figure 2.4. Mean values in upper row and standard deviations in lower row each section. Volume transport is in Sv, heat transport in TW and salt transport in $10^3 \mathrm{kgs}^{-1}$. Positive transports are eastwards in Sections A1 and A2, and northwards in Sections B, B1, B2, B3, C and D.

Section		Mass Transport			Heat Transport			Salt Transport		
No.	Name	Net	Pos	Neg	Net	Pos	Neg	Net	Pos	Neg
*A*1	Nordaustlandet-North	3.8	4.3	−0.5	37	39	−2	132	150	−18
		2.3	2.1	0.4	22	21	3	80	72	15
*A*2	North of Franz Josef	4.3	8.0	−3.7	27	27	+0	150	280	−130
		6.7	3.8	3.7	20	19	3	233	133	128
B	Svalbard-Franz Josef	−0.3	1.3	−1.7	−8	−2	−6	−12	46	−58
		0.9	0.7	0.6	6	5	7	33	23	22
*B*1	Nordaustlandet-Kvitøya	−0.4	0.1	−0.5	−1	−0	−1	−13	4	−17
		0.5	0.2	0.3	3	1	3	16	6	12
*B*2	Kvitøya-Victoria Is	0.1	0.2	−0.1	−0	−0	+0	3	6	−3
		0.2	0.1	0.1	1	1	0	6	4	3
*B*3	Victoria Is-Franz Josef	−0.1	1.1	−1.1	−6	−2	−4	−2	37	−38
		0.7	0.6	0.5	4	4	4	26	19	16
C	Edge Is-East	−0.2	+0.0	−0.2	+0	−0	1	−6	1	−8
		0.2	0.1	0.2	2	1	2	8	3	6
D	North of Hopen Trench	0.2	0.3	−0.1	−0	−0	+0	6	10	−4
		0.5	0.3	0.3	2	1	1	15	11	9

and southward mass transport were 1.1 Sv. The southward transport added 4.4 TW to the Barents Sea by transporting warm water into it, while the northward contributed 1.7 TW by transporting cold water out of it. Hence, the net 12-year mean transports through Franz Victoria Trough was 0.06 Sv and 6 TW into the Barents Sea.

In Kvitøya Strait (Section B1), southward mass transport was 0.5 Sv and northwards mass transport 0.1 Sv. Both northward and southward heat transport added heat to the Barents Sea, as for Section B3 warm water flowed southward and cold water northward, totaling to 1.4 TW also here with the largest contribution from inflow of warm water.

Section B2 from Kvitøya to Victoria Island had transports one order of magnitude smaller than Sections B1 and B3.

As a result, in the NBSO transports in Kvitøya Strait dominated the total net mass transport of 0.3 Sv, while the Franz Victoria Trough dominated the total net heat transport of 7.6 TW. The net southward salt transport of $12{\cdot}10^3 \mathrm{kgs}^{-1}$ in the NBSO was dominated by the Kvitøya Strait since the Franz Victoria Trough had large salt transports both north- and southwards that evened out in the net result.

The mean mass transport in Section C east of Edge Island was 0.2 Sv southward. Cold water was transported in both directions giving no significant net heat transport.

Section D, crossing the saddle point north of the Hopen Trench, had a mass transport of 0.3 Sv northward and 0.1 Sv southward. Cold water was transported in both directions, totaling to almost zero heat transport as for Section C.

3.3.2 Interannual variation of water mass exchange in the Northern Barents Sea Opening

Vertical section between Svalbard and Franz Josef Land

Figure 3.10 shows the yearly mean temperature and north-south velocity in the west-east vertical section between Svalbard and Franz Josef Land at 80.1°N. It shows the model gave large interannual variations in both temperature and velocity, and generally the yearly mean velocities were less barotropic than the 12-year mean velocities in Figure 3.9.

Figure 3.10 shows 1990-1992 had exceptionally warm AW with maximum extent, however reduced speed in both troughs. The conditions normalized the next years and in 1996 AW inflow reached a temporal maximum in the Franz Victoria Trough both in temperature and velocity. This year, also the cold bottom-intensified northward current on the east side of this trough increased in strength and extent.

Figure 3.10 also show the warm southward current in the Franz Victoria Trough had an upper level intensification of 6-8 cm/s on the warm (western) side in 1992-1993, 1996, and 2000-2001. The model indicated a similar current in the Kvitøya Strait in 1993-1995, 1997, and 2000-2001; this current was however on the east side of the trough. The figure depict a general cooling trend in the inflow during the 12 years, with 1997 and 1998 as the years with minimum AW inflow.

Interannual variation in transports

Figure 3.11 and 3.12 shows model mass and heat transport time series filtered with 365 days running mean giving, across Sections A1, A2, B1, B3 and B. Positions of sections are seen in Figure 2.4. Salt transports (not shown) and mass transports had almost identical interannual variation in all sections.

Figure 3.11 shows the model mass and heat transport north of Nordaustlandet (Section A1) and north of Franz Josef Land (Section A2). The main interest in these two sections is the Svalbard branch, thereby only eastward (positive) transport is shown. The eastward mass transport through Section A1 increased 2 Sv from 1992 to the end of 1994, accompanied by approximately 10 TW increased heat transport. The transports then dropped 3 Sv and 40 TW during 1995, increased slightly from 1996 to 1999, reached a local maximum of 5.8 Sv and 40 TW in 1999, and then decreased throughout the model period.

The interannual variation in eastward heat transport north of Franz Josef Land, Section A2 in Figure 3.11, resembled the fluctuations of eastward heat transport in Section A1. The corresponding mass transports showed similar trends in fluctuations, with larger amplitude of the mass transport in Section A2.

Figure 3.12 shows the model net, positive and negative mass and heat transports between Nordaustlandet and Kvitøya (Section B1; blue lines) and the Franz Victoria Trough (Section B3; green lines), and the net mass and heat transport of the whole Section B going from Svalbard to Franz Josef Land (red line). The figure shows north and southward mass transport in the Franz Victoria Trough had little variation and was almost equally large throughout the model period, resulting in a net mass transport close to zero all years. The heat transport in the Franz Victoria Trough was dominated by southward transport of warm water ($T > T_{ref}$) from 1990 to 1995, contributing about 5 TW more to the net heat transport than the northward transport of cold water ($T < T_{ref}$) these years. Southward heat transport then declined from 6 to 2 TW getting similar values as the northward heat transport during 1995 and 1996. In 1997 and 1998 southward heat transport had its minimum, and then increased slightly during autumns 1999 and 2000.

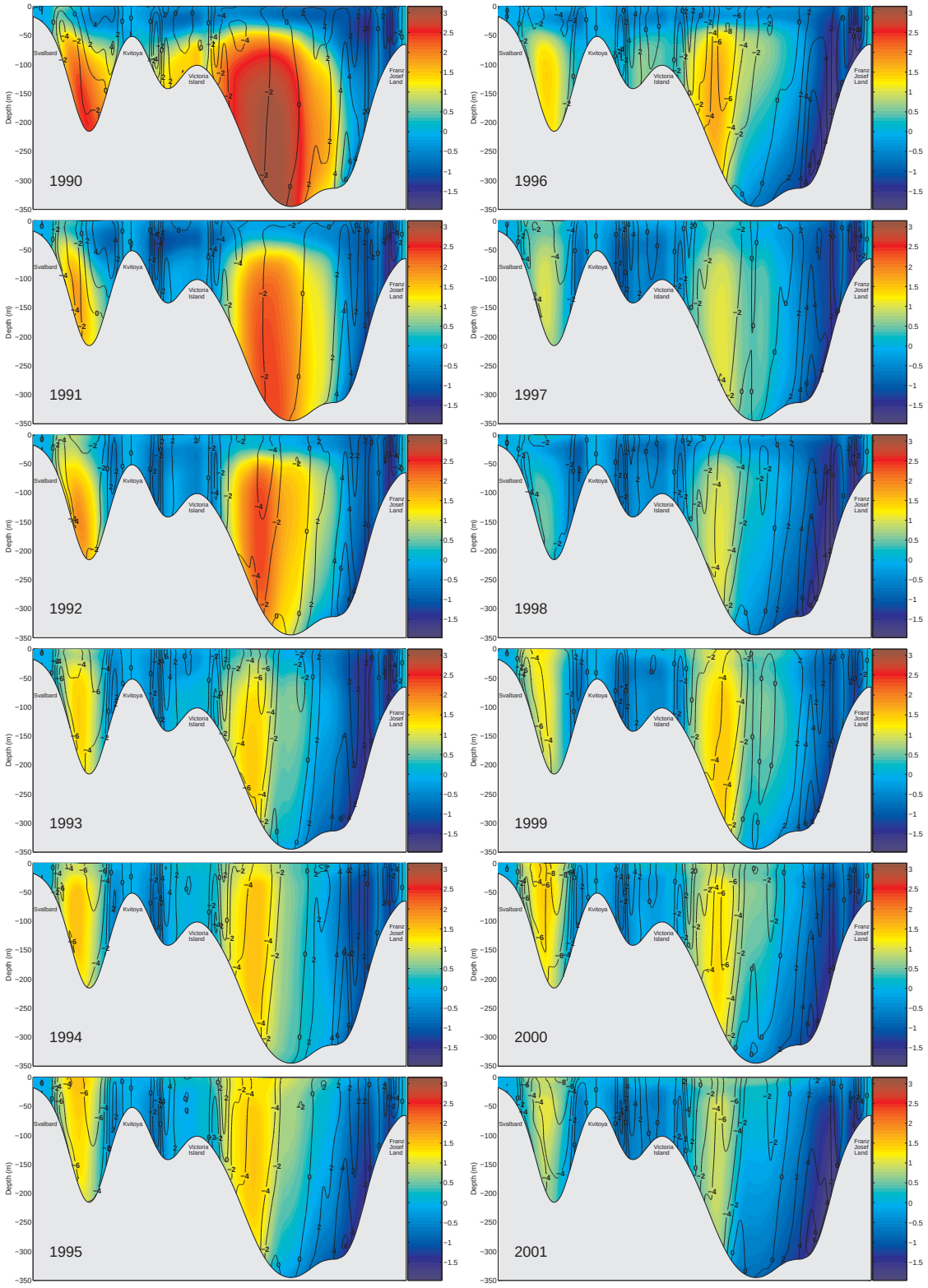

Figure 3.10: Svalbard-Franz Josef Land west-east section at 80.1°N. Yearly mean temperature (colorbar in °C) and velocity normal to the section (contours in cm/s) extracted from ROMS results. Positive velocities are northward and negative southward.

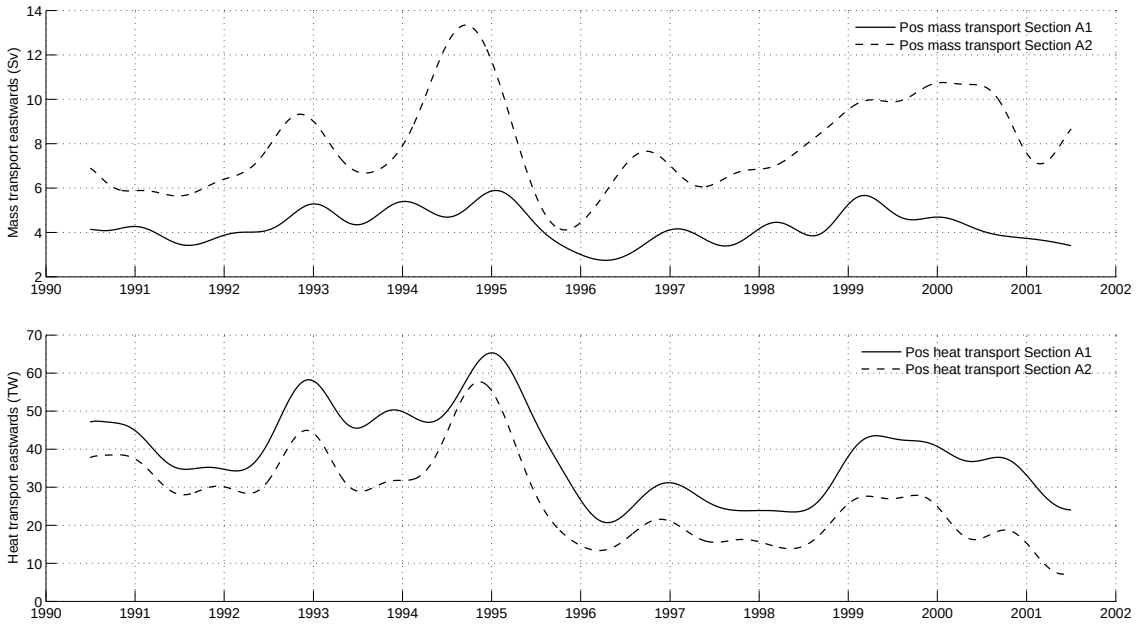

Figure 3.11: Model eastward (positive) mass and heat transport north of Nordaustlandet Section A1 (filled line), and north of Franz Josef Land Section A2 (dashed line). 365 days running mean 1990-2001. The net transports are not shown, only the positive/eastward.

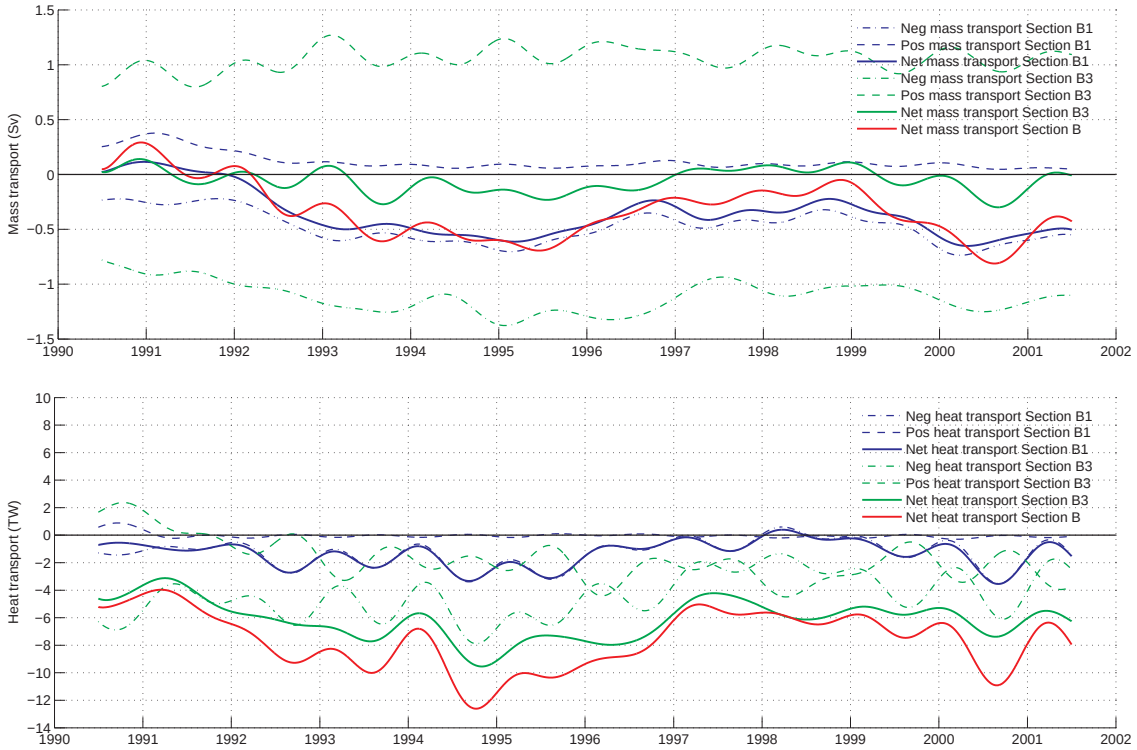

Figure 3.12: Modelled mass and heat transport between Nordaustlandet and Kvitøya Section B1 (blue lines) and between Victoria Island and Franz Josef Land Section B3 (green lines). Net mass and heat transport between Svalbard and Franz Josef Land (red line). 365 days running mean 1990-2001. Thick filled line is net transport, dashed line is northward transport (positive flux), and dash-dotted line is southward transport (negative flux).

Figure 3.12 showss the southward mass transport in the Kvitøya Strait (Section B1) was one order of magnitude larger than the northward all years except 1990 and 1991. From 1992 net mass transport followed closely the southward and was larger than average from 1993 to 1995 and in 2000. Net heat transport in Section B1 was determined by the southward flow, as northward heat transport was zero all years except 1990. It had a slight increase in 1992-1995, was nearly gone from end of 1996 through 1998, and increased again the last years having its maximum of 3.5 TW in autumn 2000.

Comparing Figure 3.11 and 3.12, the interannual variations showed some similarities, especially in 1995 and 1996 when all transports decreased.

Sections B1, B2 and B3 covered the opening between Svalbard and Franz Josef Land (Section B). Section B2 between Kvitøya and Victoria Island had mass and heat transports almost indistinguishable from zero all years (not shown). Figure 3.12 showss net mass transport in the NBSO followed closely the net mass transport in Kvitøya Strait with Franz Victoria Trough introducing seasonal fluctuations. The net heat transport of the NBSO was mainly determined by transports in Franz Victoria Trough throughout the period, with Kvitøya Strait amplifying the interannual variation.

Chapter 4

Discussion

4.1 Validation of ROMS in the northern Barents Sea

Knowing the limitations of a numerical model is crucial for reasonable interpretation of it. Here, the validity of the 9 km resolution ROMS simulation forced with ERA-40 is indicated by investigating discrepancies from observed hydrography in the northern Barents Sea. First, a brief presentation of the validity of previous simulations of the Barents Sea, a mass and heat budget for the Barents Sea, a discussion on the atmospheric forcing and other remarks about the validity of this ROMS simulation are given.

4.1.1 Aspects related to the validity of ROMS

Known limitations of ROMS

Budgell (2005) discussed the validity of a similar ROMS simulation forced with NCEP/NCAR Reanalysis. He found excessive model inflow of AW through the BSO responsible for higher temperatures and lower sea ice concentrations in the central Barents Sea than observed. The model gave a net inflow of 3.2 Sv through the BSO, which agreed well with the 3.3 Sv given by a 20 km resolution ROMS simulation which was also NCEP/NCAR forced (*Lien et al.*, 2006).

Additionally, *Budgell* (2005) reported too much ice melt in the northern Barents Sea was simulated during summer, caused by low cloud cover fraction in the simulation, even though this was modified to the monthly mean cloud cover climatology (1983-2002) of the International Satellite Cloud Climatology Project (ISCCP). He also stated the agreement between observed and modelled salinities were not as good as for temperature which in general were excellent, and that discrepancies with observations could largely be accounted for by uncertainties in the forcing fields.

Gammelsrød et al. (2008) compared two numerical models with current meter and hydrographical observations in 1991-1992 in the BSX. The models were the ROMS simulation used in this thesis and the NAME simulation used by *Maslowski et al.* (2004); *Kwok et al.* (2005). Both models were forced with ERA-40 and had 9 km resolution. Only ROMS included tides.

Gammelsrød et al. (2008) found good agreement in the velocity field of the two models, however a cold bottom intensified outflow observed on the southern side of the strait was not seen in the model results. Except for the bathymetry related differences from the observed current fields, *Gammelsrød et al.* (2008) concluded they could not say the models fail to reproduce realistic current fields.

Their observations indicated half the net mass transport to the Arctic was CBW. As ROMS simulated mainly CBW outflow and NAME had mostly AW outflow, this may indicate ROMS water mass modifications in the Barents Sea are more satisfying than NAME. *Gammelsrød et al.* (2008) argue this is caused by the NAME model not including tides, as tides induce divergence in the open ocean and effectively open polynyas particularly near coasts and islands, both effects enhancing sea-air heat exchange. *Harms et al.* (2005) found tides are important for Barents Sea heat fluxes in their sensitivity studies. Additionally, *Gammelsrød et al.* (2008) stated discrepancies from observations appeared mainly from coarse representation of bottom topography.

Mass and heat budget for the Barents Sea

The total inflow of mass through the BSO was estimated 2.8 Sv combining current measurements (1.8 Sv in the Bjørnøyarenna) and model results (1 Sv in the Norwegian Coastal Current) (*Skagseth et al.*, 2008). *Gammelsrød et al.* (2008) found a net outflow of 2.0 ± 0.6 Sv through the BSX. The mass transport in the NBSO has been estimated one order of magnitude smaller; *Maslowski et al.* (2004) reported a 23-year mean NAME estimate of 0.36 Sv into the Barents Sea through this opening, consistent with 0.33 Sv net southwards mass transport found in this study. This is also comparable to estimates from Russian literature, which is 0.1 Sv northward and 0.4 Sv southward according to *Loeng et al.* (1997).

This totals to a net mass inflow of 1 Sv, an estimate of the flow in other openings such as between Novaya Zemlya and Russia, reported 0.6 Sv out of the Barents Sea by *Loeng et al.* (1997). Mean influx of sea ice through the NBSO was estimated 14.9 mSv by *Kwok et al.* (2005) which is insignificant for the Barents Sea mass budget. It is however a major contribution to the freshwater content together with the Norwegian Coastal Current.

Net heat transport ($T_{ref} = 0.1°\mathrm{C}$) into the Barents Sea between Norway and Svalbard was estimated 73 TW by *Gammelsrød et al.* (2008) and 65 TW by *Maslowski et al.* (2004). *Skagseth et al.* (2008) report 48 TW inflow based on the current meter array in the BSO. *Gammelsrød et al.* (2008) found a net heat transport into the Barents Sea through the BSX of 3.6 TW calculated from moored current instruments, 5.6 TW in ROMS results and 7.4 TW out of the Barents Sea in NAME results. According to *Maslowski et al.* (2004) NAME gave a 23-year mean net heat transport of 2.2 TW out through the BSX. They also found a net heat transport in the NBSO insignificantly different from zero (0.76 TW). Table 3.3 shows ROMS gave a net heat transport of 7.6 TW into the Barents Sea, with the largest contribution from inflow of AW (5.6 TW) and partly from outflow of cold water (2.0 TW), both predominantly through Franz Victoria Trough.

The results from ROMS total to a net heat transport of 86 TW into the Barents Sea, significantly smaller than the average heat loss to the atmosphere estimated 140 TW by *Simonsen and Haugan* (1996).

Atmospheric forcing fields

The NCEP/NCAR Reanalysis has more incoming shortwave radiation at the surface of the Barents Sea than the atmospheric forcing fields ERA-40, SRB V2 and ISCCP POLAR (A. Sorteberg, personal communication). This difference is largest in June (100 Wm^{-2}) and decreases to zero in the winter when incoming shortwave radiation vanishes. Similar comparisons show ERA-40 has 10 to 30 Wm^{-2} more incoming longwave radiation at surface than NCEP. The large difference in incoming shortwave radiation between NCEP

and ERA-40 indicate summer ice melt in this ROMS simulation with ERA-40 is less than the excessive ice melt reported by *Budgell* (2005).

It is possible the daily mean wind stresses in NCEP are too high (*Budgell*, 2005). *Renfrew et al.* (2002) compared reanalysis from NCEP and the ERA Project with observations and found the roughness length formula used in NCEP is not suitable for moderate to high wind speeds, especially in regions with large air-sea temperature differences and high wind speeds such as the Barents Sea. This could produce an over-estimate of wind stress during storm events, conditions favourable for inflow through BSO (R. Ingvaldsen, personal communication) (*Budgell*, 2005). *Renfrew et al.* (2002) concluded surface flux fields from ERA-40 are within the bounds of observational uncertainty and suitable for forcing ocean models. Additionally they stated NCEP reanalysis surface fluxes are not suitable for this purpose due to overestimates of sensible and latent heat fluxes.

However, this study show indications of excessive inflow of AW through the BSO also in this ERA-40 forced ROMS simulation, see Figure 4.2. Additionally, there are discrepancies in the Svalbard branch, possibly caused by too strong flow and/or too warm AW which could be attributed to the atmospheric forcing field.

Gammelsrød et al. (2008) found the ROMS ERA-40 hindcast having too high heat content in the Barents Sea interior (0.60°C bias (model too high) in Kola section at 33°30'E). This can cause too much ice melting and thereby higher rate of heat loss to the atmosphere in the Barents Sea. *Budgell* (2005) found a similar bias of 0.63°C in the Kola section in the for the NCEP hindcast of ROMS.

Harms et al. (2005); *Gammelsrød et al.* (2008) argue the choice of atmospheric forcing has a larger influence on the model results than the choice of model, and *Gammelsrød et al.* (2008) found larger differences between the ROMS simulations forced with NCEP and ERA-40 than between the ROMS ERA-40 and NAME ERA-40 hindcast.

Initial value problem

Figure 3.10 the first two years of the model period had exceptionally warm and broad inflow of AW in the Franz Victoria Trough and extended northward flow in the Kvitøya Strait. Horizontal fields of temperature and salinity in 1990 (not shown) revealed the northern Barents Sea was significantly fresher than the 12-year mean and inflow of AW from north reached unusually far south.

These can be signs of an initial value problem for the regional Barents model (see Chapter 2.2.1 for details of ROMS set up). However, Figure 3.3 shows observed currents west of Kvitøya 1980-1983 were northeastwards, and the model gave a comparable flow in 1990-1991. This may also indicate the dynamical regime dominating the northern Barents Sea in 1990-1991 was similar to that in 1980-1983, giving increased northward flow, and then shifted in 1992.

It is worth noticing *Budgell* (2005) ignored the first year 1990 as a spin up year when calculating the bias in the NCEP forced ROMS simulation relative to observed temperatures in the Kola section.

Topographic steering

Figure 3.8 shows ROMS gives topographically steered currents. Observations in Figure 4.2 show AW intrudes the Barents Sea from north crossing the Kvitøya Bank while ROMS only allow AW to flow around the bank, following its isobath. This may signal ROMS has enhanced topographic steering.

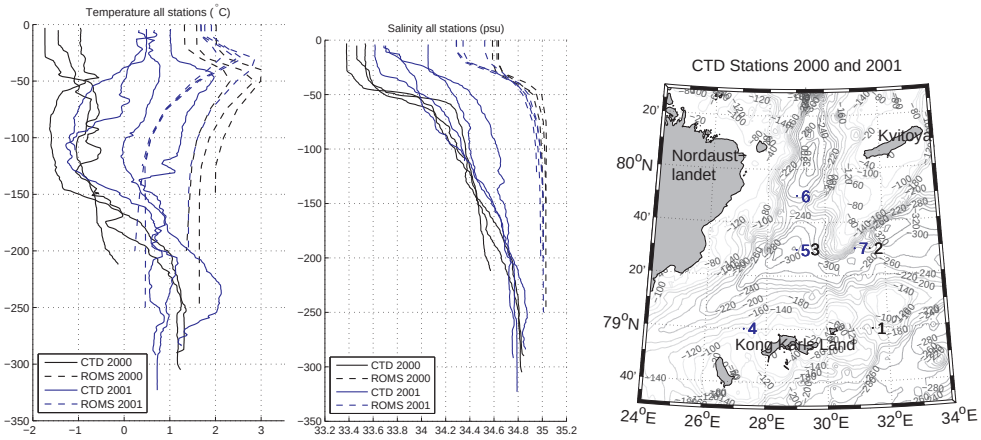

Figure 4.1: Observed and modelled temperature (left) and salinity (middle) in the region of Kong Karls Land at positions in map (right). Three CTD stations Sept 30 2000 (blue thick lines) are shown with corresponding modelled profiles (blue dash-dotted lines), and four CTD stations Sept 30 2001 (black thick lines) with corresponding modelled profiles (black dash-dotted lines).

The bathymetry of ROMS is smoother than the real, lacking roughness that can produce boundary layer turbulence and flow perturbation, possibly a reason for this discrepancy.

The first baroclinic Rossby radius of deformation in the northern Barents Sea was calculated 3 km from observations by *Løyning* (2001), indicating the length scale of baroclinic eddies in this region. Accordingly this ROMS simulation with 9 km horizontal grid resolution does not resolve eddies of this scale.

4.1.2 Comparing with observed hydrography in the northern Barents Sea

Arctic Water missing in autumn north of Kong Karls Land

Figure 4.1 shows seven CTD stations north of Kong Karls Land September 30 2000 and 2001 with modelled temperature and salinity profiles the same days at corresponding grid points.

The comparison shows ROMS does not capture small scale variability, and gave generally warmer and more saline water masses than observed. In fact, ArW was absent in the modelled profiles and the best agreement was in 2001 when less ArW and warmer SW was observed. The resemblance was significantly better in the deeper layers. Furthermore, model halocline depth was almost identical to the observed, although the observed was sharper and spanned a greater salinity interval.

Discrepancies from observations were equal or worse in profiles one month before and later. Other grid points northwest and south of Kong Karls Land were tested against observations and had similar disagreements (not shown). Model profiles in the Storbanken region were however colder and more similar to the observed temperatures north of Kong Karls Land.

Model profiles August 15 2000 and 2001 (not shown) demonstrated the model temperature maximum at 40 to 50 m depth in Figure 4.1 originated from summer surface warming followed by cooling in autumn. The observation in the Kvitøya Strait had a similar temperature profile as the model profiles. This may indicate ROMS simulates better the inflowing AW than water mass modifications inside the Barents Sea.

Since ROMS gave cooling below -0.1°C of the whole water column north of Kong Karls

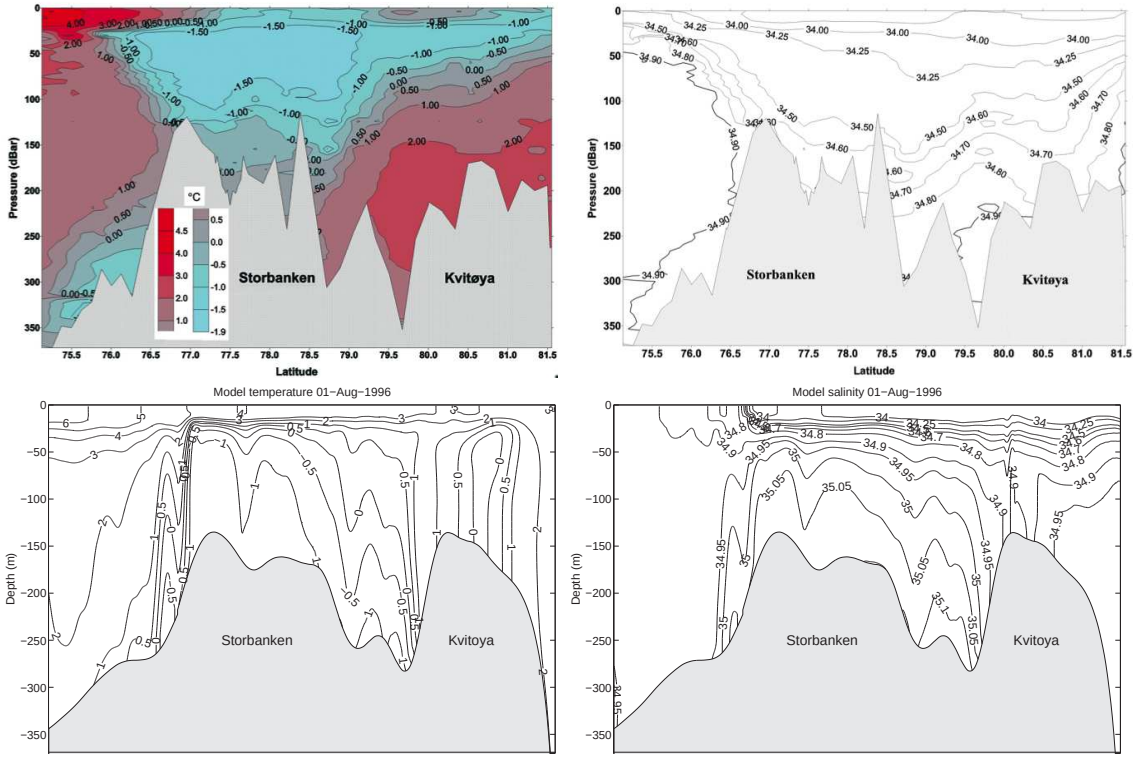

Figure 4.2: Observations published by *Løyning* (2001) (upper figures) in a north-south going section at approximately 35°E July-August 1996, see map in Figure 2.1. Corresponding model vertical fields August 1 1996 (lower figures). Temperature in left figures, salinity in right.

Land during winter (not shown), absence of ArW in this comparison could be caused by too intensive summer heating in ROMS. Salinities were however still too high for ArW, ranging from 34.9 to 35.2 psu.

Modelled and observed Atlantic Water north and south of Storbanken

Figure 4.2 shows temperature and salinity in a north-south going section at approximately 35°E observed July-August 1996, published by *Løyning* (2001), and the corresponding model section August 1 1996.

The observed section show AW intruding the region north and south of Storbanken, the northern 1°C warmer and 0.2 psu fresher than the southern. On Storbanken, ArW was observed with a temperature minimum of −1.5°C at 50 m depth extending northwards above the AW. At the bottom on Storbanken a small temperature increase was observed, and CBW was observed near the bottom on the southern slope of Storbanken.

ROMS simulated AW both north and south of Storbanken. The spatial distribution of the northern AW was however very different from the observed as no AW appeared on the Kvitøya Bank. Instead, as mentioned earlier Figure 3.8 a) shows ROMS only allow AW to follow the topography around the Kvitøya Bank.

Figure 4.2 also shows the model gave cold water on Storbanken with too high salinity making it denser than the AW. Additionally, observed cold bottom water south of Storbanken appeared in ROMS both north and south of Storbanken. These discrepancies indicate exaggerated CBW formation from ice growth in ROMS. If the model enhances topographic steering as discussed in Chapter 4.1.1, water may circulate and stay on Storbanken being exposed to increased salinification for a longer time than reality.

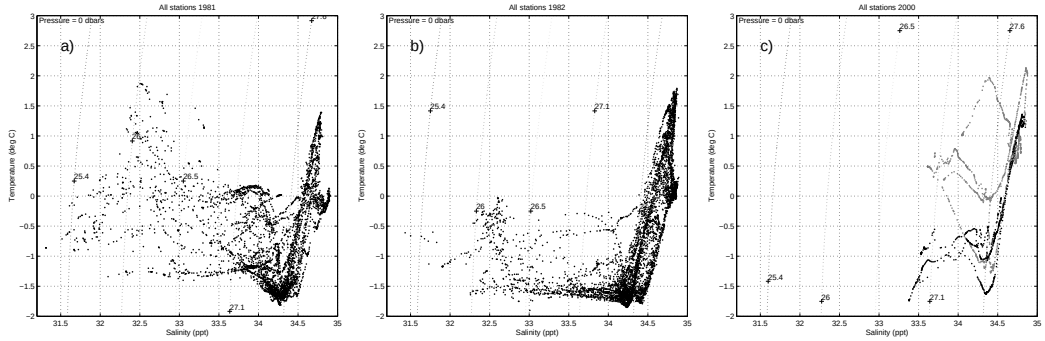

Figure 4.3: Temperature-salinity profiles of CTD stations on map in Figure 2.1; Stations 333-335 north of Nordaustlandet excluded. Observations from August 1981 a), August 1982 b), September 30 2000 - black dots in c) and September 30 2001 - gray dots in c).

Closer agreement for Atlantic Water

Figure 4.1 indicate the model gave a more correct vertical distribution of salinity than of temperature even though the salinity was too high throughout the water column. Both temperature and salinity agreement was much better for AW than SW and ArW. It is noteworthy the model had almost identical temperature profile as one observation in the region of AW inflow in the Kvitøya Strait. Figure 4.2 also indicates the model AW is in closer agreement with observations than ArW.

Atlantic water descents under Surface Arctic Water too far east

Figure 3.7 shows AW in the Svalbard branch appears at the surface until it reaches approximately 40°E in this ROMS simulation. *Schauer et al.* (1997) observed hydrography on the northern Barents Sea shelf edge at 30°E and found cold, low-salinity water above the AW. This discrepancy indicates AW in ROMS extend too high up in the water column when entering the northern Barents Sea, and probably contributes to ROMS having warmer water masses than observed as seen in Figure 4.1. Other possibilites for the water massses in Figure 4.1 being too warm could be too high temperatures of AW in the Svalbard branch and/or too high velocities in this current bringing warm water too far into the Barents Sea.

4.2 Distribution and circulation of water masses in the northern Barents Sea

4.2.1 Observed water masses and indications of their natural variability

Figure 4.3 shows temperature-salinity profiles of the CTD observations seen on map in Figure 2.1, Stations 333-335 north of Nordaustlandet excluded.

Figure 4.3 a) and b) of observations in 1981 and 1982 respectively, show two cores within the definition of ArW. They had salinity 34.25 and 34.5 psu and were both close to freezing point temperature. Two temperature maxima in the range of AW were also seen in 1981 and 1982, one warmer than 1°C and salinity 34.8 psu, the other one from 0 to 0.3°C and salinity 34.9 psu.

Figure 4.4 compare CTD stations observed different times at approximately the same position. This comparison may indicate natural short time variability but is not expected to reflect any interannual variation.

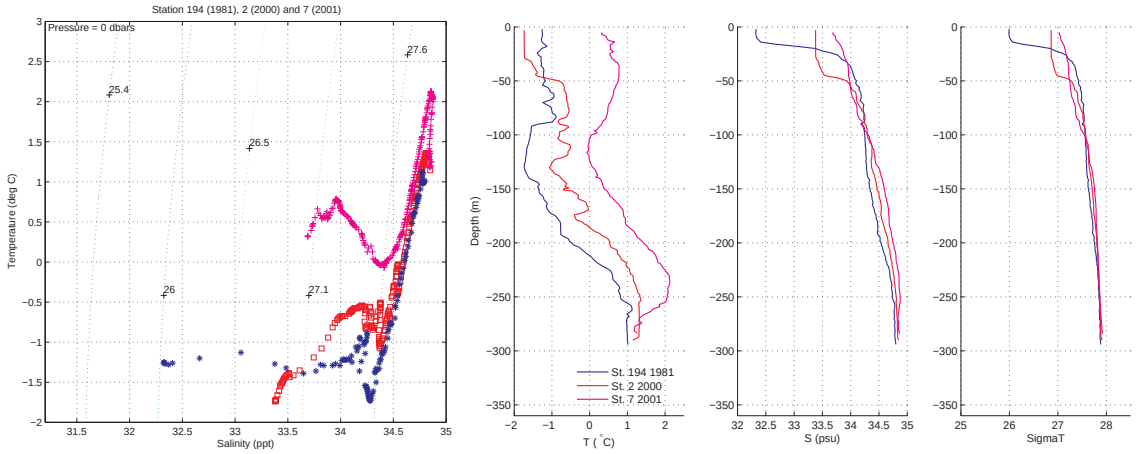

Figure 4.4: Temperature-salinity and vertical profiles of CTD stations at approximately the same location observed at different times. Station 194 August 27 1981, Station 2 September 30 2000 and Station 7 September 30 2001 at the deepest region in section between Kvitøya and Kong Karls Land, see map in Figure 2.1. Temperature-salinity profiles a), vertical profiles of temperature b), salinity c) and density d).

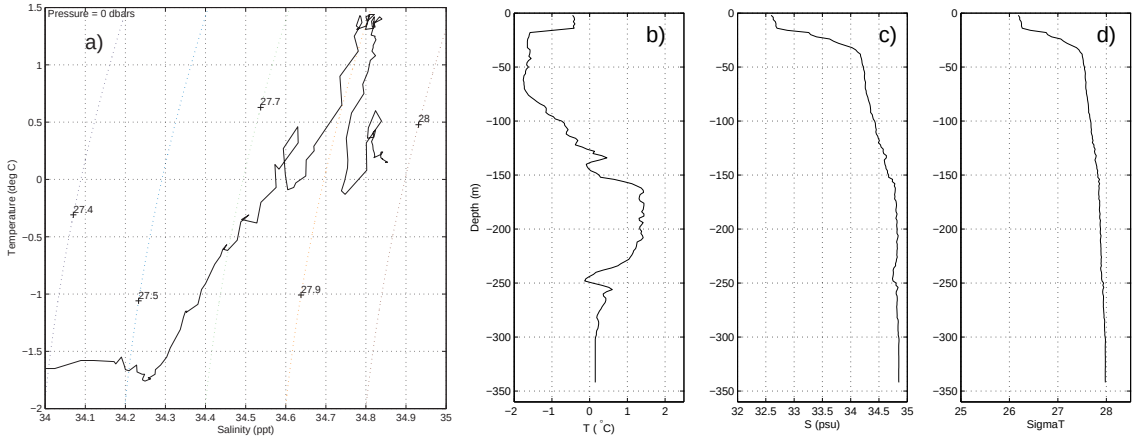

Figure 4.5: Temperature-salinity diagram focused on Arctic and Atlantic Water a), and vertical profiles of temperature b), salinity c) and density d) of Station 278 observed August 21 1982 northeast of Storbanken, see map in Figure 2.1. Three temperature maxima are seen in the profile, possibly reflecting the meeting of two Atlantic water masses, one flowing above and below the other.

The figure shows Station 194 in 1981, Station 2 in 2000 and Station 7 in 2001 in the narrow channel between Kvitøya and Kong Karls Land, see map in Figure 2.1. The temperature profiles differed more than salinity profiles which were almost identical in the whole water column except the surface layer. The deep region's temperature difference could be attributed to increased AW inflow in September. It is interesting to note bottom layer temperatures were almost identical (1°C) for these stations 20 years apart.

Similar comparisons were made for other stations (not shown). These indicated salinity vary less than temperature, and the largest variations are seen in the surface layer probably due to large sensitivity to atmospheric and sea ice conditions.

Atlantic Water from north meets transformed Atlantic Water from south

Figure 4.5 shows the temperature-salinity and vertical profiles of Station 278 observed northeast of Storbanken August 21 1982, see position on map in Figure 2.1. The temperature-salinity profile in Figure 4.5 a) shows three pronounced temperature max-

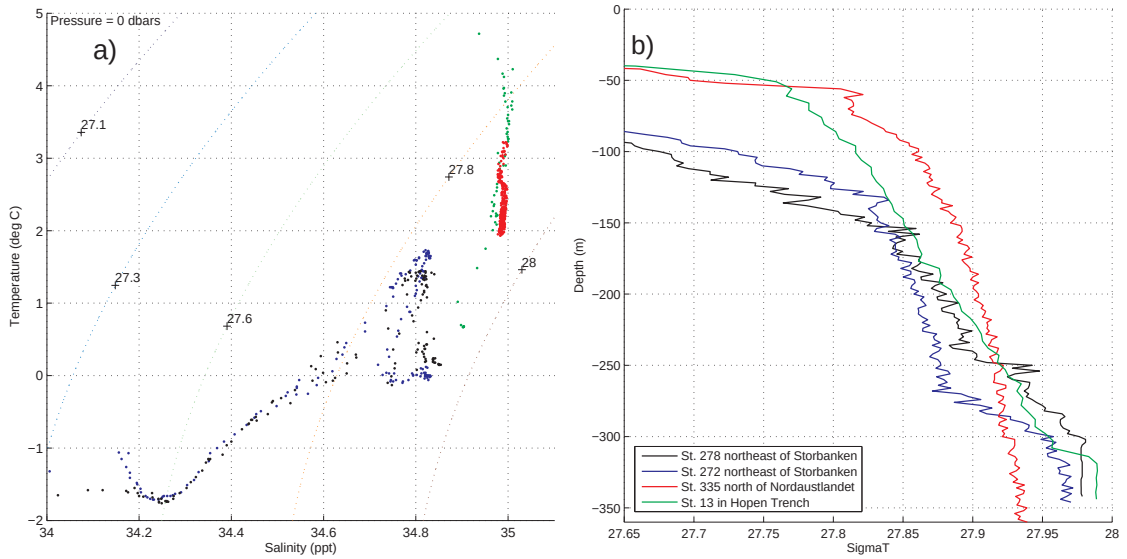

Figure 4.6: Temperature-salinity diagram a) and vertical density profiles focused on deeper parts b) of four selected CTD stations taken late August 1982: Station 335 north of Nordaustlandet (red), Stations 278 (black) and 272 (blue) on the northeastern edge of Storbanken, and Station 13 in Hopendypet (green). Positions of Stations 335, 278 and 272 are seen on map in Figure 2.1.

ima in the range of AW accompanied by increased salinity. The ArW core formed a straight mixing line - indicating local mixing processes were important - with the temperature maximum at 0.5°C and 34.6 psu. Figure 4.5 b) shows this maximum was situated at 130 m depth, and that the warmest maximum spanned from 160 to 220 m depth, reaching 1.5°C and 34.8 psu. The deep maximum at 260 m depth had similar salinity as the warmest maximum and temperature comparable to the upper maximum.

Figure 4.6 b) emphasize the deep density profile of Stations 278 and 272 northeast of Storbanken, Station 335 north of Nordaustlandet and Station 13 in Hopen Trench, all observed August 1982.

The density at Station 278 increased linearly with depth, however the rate of density change was altered at two depths. This gave a three-step structure: Two depth intervals with rapid changing density were separated by a depth interval with slower change. Additionally, the homogenous bottom boundary layer was seen below 300 m. The same structure appeared and was more prominent at Station 272, situated nearer the Franz Victoria Trough. Interestingly, the depths of altered rate of density change - 150 and 250 m depth - also separated the three temperature maxima in Figure 4.5 b).

The observed profile could be the signature of AW entering from north through Franz Victoria Trough meeting transformed AW originating from the BSO. Observations by *Løyning* (2001) in Figure 4.2 shows this could occur if AW from south manages to flow around or across Storbanken. Figure 4.6 a) shows the density of the warmest maximum at Station 278 was encompassed by densities of AW north of Nordaustlandet (Station 335) and in Hopendypet (Station 13).

Figure 4.6 b) also shows the density profile of AW north of Nordaustlandet was steeper than in Hopendypet. The two profiles had equal density at 250 m depth. Above and below this depth, AW in Hopendypet was lighter and heavier than AW north of Nordaustlandet, respectively. If the two water masses met, AW from south would flow above and below, leaving AW from north in the middle. Hence a temperature profile as seen in Figure 4.5 b) could form.

It is however also possible the transformed AW originates from north, as AW entering

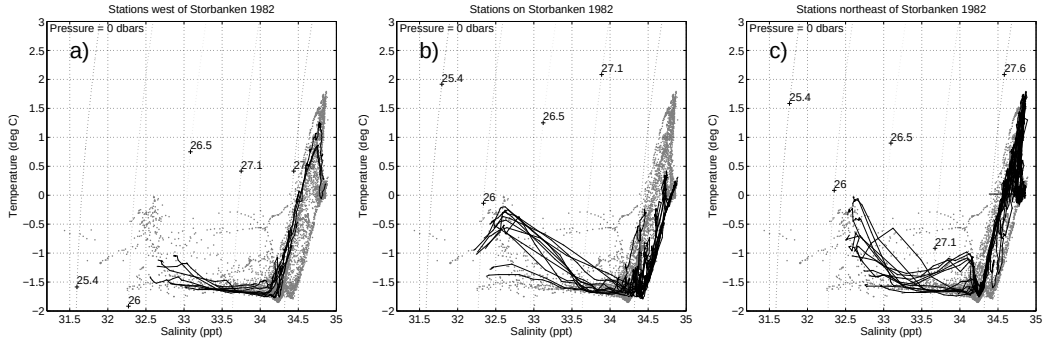

Figure 4.7: Temperature-salinity profiles of CTD stations observed August 1982 (grey dots; similar in a), b) and c)), and stations from different regions around Storbanken highlighted as black lines in each figure: West of Storbanken (Stations 302-310) a), on the northwestern slope of Storbanken (Stations 288, 291-301) b) and northeast of Storbanken (Stations 272-284) c). Positions of stations are seen on map in Figure 2.1

through the Franz Victoria Trough continues toward Kong Karls Land and circulates back along the northeastern edge of Storbanken, being cooled and mixed with ArW in its way.

The most suitable observations were chosen for this discussion.

Interestingly, *Maslowski et al.* (2004) showed an observation from the St. Anna Trough in their Figure 8 b) with remarkably similar temperature-salinity profile as Figure 4.5 a). In this region AW modified in the Barents Sea meets AW in the Svalbard branch.

Different mixing lines on and around Storbanken

The fresher ArW core in Figure 4.3 a) and b) generally mixed with the freshest and warmest AW, while the more saline ArW core mixed with the more saline and denser AW. Figure 4.7 divides temperature-salinity profiles of CTD observations in 1982 in those between Kong Karls Land and Storbanken a), on the northwestern slope of Storbanken b) and northwest of Storbanken c). Figure 4.7 b) shows the more saline mixing lines between ArW and AW were on the northwestern slope of Storbanken. Figure 4.7 c) shows the warmest AW was measured northeast of Storbanken and mixed with the fresher ArW core. This AW also mixed with the denser, colder and more saline AW core below. Figure 4.7 a) shows the freshest mixing line appeared in the deep region between Kong Karls Land and Storbanken, where the fresher ArW core mixed with 1°C AW that also mixed with colder and more saline AW below.

Modification of Surface and Arctic Water form Cold Halocline Water

Cold Halocline Water (CHW) was first mentioned by *Aagaard et al.* (1981) as the water mass separating cold surface water from underlying warm AW in the Arctic Ocean. They concluded CHW can not be formed in the Arctic Ocean and suggested it is formed in the adjacent shelf seas and advected into it. They defined CHW as water colder than -0.5°C and salinity between 34 and 34.5 psu, a definition also applied by *Steele et al.* (1995) and *Løyning* (2001).

Questions arise as to which water masses and processes contribute to formation of CHW, where it is formed and where advection to the Arctic Ocean occur.

Aagaard et al. (1981) proposed upwelling of AW on the shelfs could produce CHW by freshening from melting sea ice and cooling by the atmosphere, as they observed on the shelf of the Alaskan Beufort Sea. They also proposed a second possible mechanism, namely salinization of shelf water during sea ice formation. *Løyning* (2001) did not find

any sign of upwelling of AW on the northern shelf of the Barents Sea, however he observed modifications of Arctic and Atlantic Water on Storbanken and south of Kvitøya pointing directly towards the CHW definition.

AW is not observed upwelling to the surface in the Barents Sea, neither in previous publications nor here. However, *Kowalik and Proshutinsky* (1995) demonstrated in their numerical studies of tidal and topographic interaction around Bjørnøya that AW may upwell to the surface layer here. Additionally, AW flowing in through the BSO is situated high up in the water column and may meet the ice edge, possibly producing CHW by modifications of AW as discussed by *Steele et al.* (1995).

Modifications of Surface and Arctic water is suggested the primary mechanism for CHW formation in the northern Barents Sea since this occurs to a great extent in observations and model results presented here. This happens more extensively on banks since the water column here is shallower, meaning the released brine from sea ice formation is spread in a smaller volume, and because the anticyclonic circulation on and around the banks keep the water masses exposed to this increased salinification for a longer time.

Løyning (2001) also suggests the cooled AW observed close to bottom on Storbanken in 1981, 1982 and 1996 is caused by horizontal and vertical currents induced from interaction between bathymetry gradients and tidal motion as discussed by *Kowalik and Proshutinsky* (1995). The observations in Figure 4.7 supports this as the water close to bottom in Storbanken had similar TS-properties as the bottom water northeast of Storbanken. It is suggested AW on Storbanken simply mix with the CHW above through local mixing processes, indicated by the straight mixing line between the two water masses. This colder denser AW was proposed as AW originating from southern Barents Sea by *Pfirman et al.* (1994). However, the properties of the transformed AW from south are not easily distinguished from the bottom water, discussed below.

Polynya activity produce Cold Bottom Water

Midttun (1985) defined Cold Bottom Water (CBW) colder than $-1°C$ and salinity above 34.95 psu. He reported observations of CBW in deep regions near Novaya Zemlya and Spitsbergenbanken, and outflow of CBW south in BSX.

Additionally, *Schauer et al.* (1997) suggested cold dense water drain out the Franz Victoria Trough based on their observations north of the Barents Sea. Figure 3.9 show the model gave cold outflow near the bottom at the east side of Franz Victoria Trough, and the temperature field at 200 m depth in Figure 3.7 shows cold water along the slope west of Franz Josef Land.

Winsor and Björk (2000) found extensive dense water production in a polynya south of Franz Josef Land, supported by HAMSOM results by *Harms* (1997). It is likely this water flow down along the slope, some of it ending up in the depression south of Franz Josef Land. A larger polynya frequently occurs west of Novaya Zemlya, producing dense water filling the Northeast Basin. Figure 3.7 shows the model gave cold saline water in these two depressions and a depression east of Storbanken; the coldest dense water south of Franz Josef Land with $-1.7°C$.

Figure 3.2 shows the regions west and northeast of Storbanken had a water mass slightly warmer than CBW at the bottom. *Pfirman et al.* (1994) suggested this water mass as transformed AW from south. The temperature profile of Station 278 northeast of Storbanken in 1982, Figure 4.5 b), shows a temperature increase at 260 m depth and a homogenous colder bottom layer below. If remnants of CBW from the depressions formed during winter, may flow along the bottom and mix with transformed AW from south lying above, this could form the observed bottom water mass. The salinity of the transformed

AW from south and CBW is highly similar, meaning a mixture of the two would only warm the CBW, consistent with observations.

Figure 3.4 a) shows the upper current meter east of Kvitøya may have observed CBW production, as water with temperature close to freezing point and salinity 35.2 psu was measured in March, April and May 1981. It is also interesting to note the week in July 1981 with CBW characteristics occurring at the same time as an exceptional westward current component, possibly cold dense water transported off the shallow area around Kvitøya.

Water mass circulation in the northern Barents Sea

The model flow field is described in Chapter 3.3.1. Conservation of potential vorticity gave topographically steered currents. Additionally, the model currents were highly barotropic, however to a less degree in the yearly mean fields compared with the 12-year mean. This is seen as the velocity contour lines in Figure 3.10 of the yearly mean velocity between Svalbard and Franz Josef Land are less vertical than in the 12-year mean in Figure 3.9.

The model gave the most distinct baroclinic current between Nordaustlandet and Kvitøya in 1990 and 1991, see Figure 3.10. These years, an increased northward flow intensified at the surface occurred on the east side of the strait, possibly indicating it was wind induced, with a southward current below.

The observed northeastward current west of Kvitøya 1980-83 in the cold ArW core (Figure 3.3) coincided with the modelled cold northward flow at the east side of the Kvitøya strait seen in Figure 3.9. However, the northward flow of warm saline AW close to the bottom was modelled southwards all years. During 1990 and 1991 the northward modelled flow was broader and intensified, with water warmer than 0°C down to 150 m depth. If the dynamic regime of the northern Barents Sea during the current observations in 1980-83 was similar to 1990-91 and this regime shifted toward a different regime during 1992, observed and modelled current could be coherent in the strait.

Most of the model flow is completely different from previous interpretations of the northern Barents Sea flow by e.g. *Loeng* (1991); *Pfirman et al.* (1994); *Loeng et al.* (1997); *Gammelsrød et al.* (2008). The exception is inflow of AW through Franz Victoria Trough which has been mentioned earlier. However, this flow was assumed to flow out again west of Kvitøya, which here is seen only to occur to a very small degree the first two years of the model period, and with a small velocity in the lower current meters 1980-1983 seen in Figure 3.3. Instead, ROMS gives AW circulating in the northern Barents Sea loosing its heat content by mixing with ArW above and possibly colder AW or AW mixed with CBW below.

The largest flow discrepancy in this thesis from previous publications is the flow on the northwestern slope of Storbanken which the model indicate northward and previously has been interpreted southward. Additionally, no cold current is seen flowing in through Franz Victoria Trough as previously assumed, rather out of it throughout the water column on the east side of the trough, seen in Figure 3.9. This discrepancy influence the heat transport by exporting cold water out of the Barents Sea with 2 TW according to ROMS. This flux estimate is however likely too high as water mass transformations in ROMS is too extensive forming too much cold saline water as discussed in Chapter 4.1.

Abrahamsen et al. (2006) found topographically steered currents toward southeast in Olga Basin in their current meter time series from 1993-1996, consistent with the model flow seen in Figure 3.8. Temperature and salinity time series in their moorings indicated ArW above AW with origin from north, and that increased southward velocity component of the AW displaced the boundary between the two water masses, representing stronger

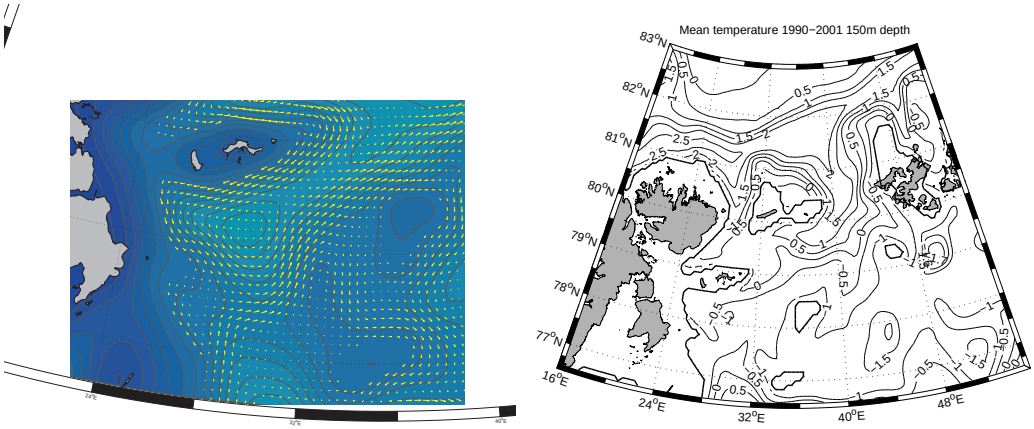

Figure 4.8: 12-year mean velocity at saddle point north of Hopen Trench 150 m depth (left) and 12-year mean temperature field at 150 m depth (right).

influx of AW from north. These observations were also consistent with *Pfirman et al.* (1994).

Cross saddle point flow in ROMS allowing AW flow from south to north

The possibility of AW flowing from Hopen Trench over the saddle point into Olga Basin is of particular interest, as this can increase the heat content of the northern Barents Sea and could explain the densest of the two distinctive AW water masses in Figures 4.3 a) and b) and 4.5. This cross-saddle point flow was suggested by *Pfirman et al.* (1994). *Harris et al.* (1998) argued no dynamical mechanisms are known to get AW up this high allowing it to cross the saddle point. *Li and McClimans* (1998) discussed the possibility of a barotropic, retrograde (topographically steered with shallow water to the left) slope jet along the southern slope of Svalbardbanken.

Figure 4.8 (left) shows the model flow at 150 m depth above the saddle point, the deepest model velocity field above this point. Here, current arrows at all grid points are shown and it is seen a flow northwards at the western slope of Hopen Trench with the slope to the right, crossing the saddle point westwards and joining the flow in Olga Basin northeastwards along the slope of Storbanken. Figure 4.8 (right) shows the model has AW at 150 m depth spanning from Hopen Trench and northwards.

The Persey Current -possibly a misinterpretation of hydrography observations

The Persey Current is not recognized in the model results. If the currents in ROMS are comparable to the reality and ROMS has the AW inflow too high in the water column (as proposed in Chapter 4.1.2), then an inflow of cold ArW from north extending southwestwards into the Barents Sea is possible. The Persey Current has been concluded from hydrographical observations showing cold ArW extending from the northeast of the Barents Sea close to Franz Josef Land to Storbanken, further toward Hopen and Bjørn oya. However, it is suggested that this water mass could originate from winter cooling from the atmosphere forming in the Barents Sea, and that the inflow of warmer water from north and south limits the extension of the ArW. If there was no inflow of AW, the whole Barents Sea water mass would cool down to -1.8°C with the present atmospheric conditions during winter and only the surface layer would heat up during summer. The reason it has been interfered like described above is natural since the inflow of AW from north and south of this region leave the coldest water in patches similar to those a current like the

Persey Current would form. Figure 3.7 of the modelled hydrography fields shows the cold water extend from Franz Josef Land southwestward across Storbanken and toward Edge Island, meaning the model also has a hydrographic field that could be interpreted as the Persey Current bringing ArW from the Arctic Ocean.

4.3 Water mass exchange with the Arctic Ocean in the region Svalbard-Franz Josef Land

4.3.1 Interpretations from model transports

Different roles of the straits in the Northern Barents Sea Opening

Table 3.3 of 12-year mean transports shows the strait between Nordaustlandet and Kvitøya determine the net mass transport through the NBSO even though mass exchange is much larger in the Franz Victoria Trough. The reason is the highly balanced mass transport in and out of Franz Victoria Trough, also seen in the interannual mass transport variation in Figure 3.12. Since the outflow in Franz Victoria Trough is cold and the inflow is warm, this water mass exchange dominate the heat transport through the NBSO.

Correspondence of Svalbard branch variation and inflow to the northern Barents Sea

Figure 4.9 shows deviations from the 12-year mean of model mass and heat transport eastward north of Nordaustlandet (Section A1) and southward between Svalbard and Franz Josef Land (Section B; NBSO). The transports are 365 days running means (Hanning window), and the deviations were normalized in order to compare their variations. Section B transports were multiplied by -1 for easier comparisons so that positive deviations in Figure 4.9 resemble larger than average transport.

The eastward mass transport north of Nordaustlandet (black filled line in Figure 4.9) was larger than average from autumn 1992 to the summer of 1995 and from the end of 1998 to spring 2000. This intensified mass flow was accompanied by increased heat transport, especially in the period 1992-1995. A correlation coefficient of 0.8 significant on a 1% level was found for the interannual variation of eastward mass and heat transport north of Nordaustlandet, meaning 64% of the interannual variation can be explained by this correlation.

It is reasonable to assume intensified mass flow in the Svalbard branch lead to increased inflow of AW through the NBSO. Figure 4.9 shows inflow increased the same periods as the Svalbard branch intensified, however with a time lag, reflected in the increased correlation coefficient from 0.2 to 0.7 when the mass inflow through the NBSO was shifted one year. Hence, the one year time lagged significant correlation of 0.7 can explain nearly 50% of the interannual variation of mass inflow to the northern Barents Sea.

Comparisons of yearly mean model hydrography fields at each depth (not shown) indicated changes in the Svalbard branch first occurred in upper layers, then propagated to deeper layers the next two to three years. Hence, these analyses may indicate the intermediate or deeper layer mass transport interannual variation in the Svalbard branch is important for interannual variation of mass inflow through the NBSO, and induces a time lag of approximately one year in the correlation.

Figure 4.9 also shows the interannual variation of heat transport southwards through the NBSO follows the interannual variation of heat transport in the Svalbard branch to some extent. Here a significant correlation coefficient of 0.6 was found, meaning 37% of the

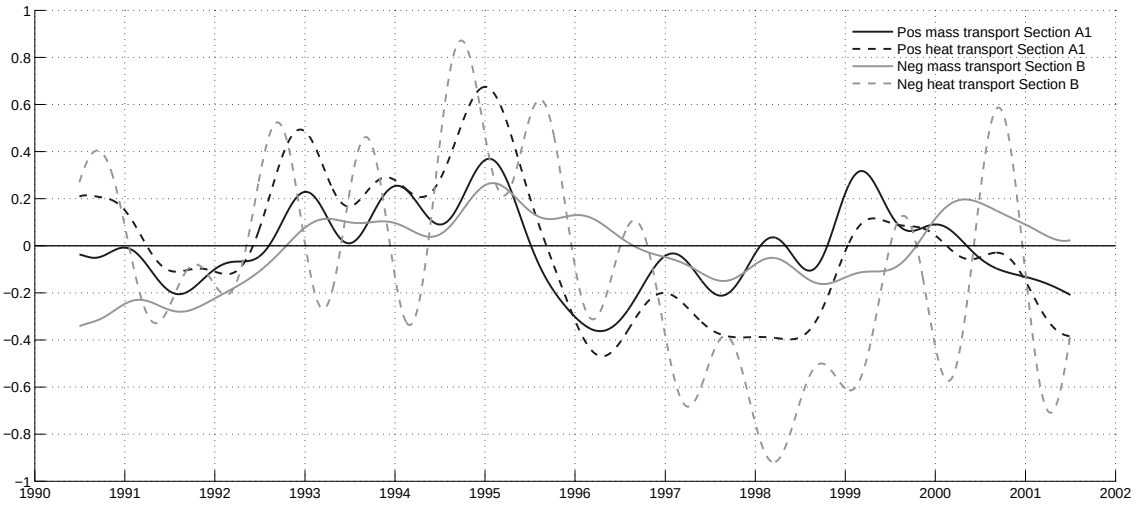

Figure 4.9: Deviations from 12-year mean of model mass and heat transport eastward (positive) in Section A1 north of Nordaustlandet and southward (negative) in Section B Svalbard-Franz Josef Land (the NBSO). Black lines are for Section A1; gray lines for Section B. Filled lines are mass transport; dashed lines are heat transport. 365 days running mean 1990-2001. Deviating transports are scaled in order to compare interannual variation. Section B transports are multiplied with −1 for easier comparisons; positive deviations are transports larger than the 12-year mean.

interannual variation of heat transport southward through the NBSO could be explained by this correlation.

This comparison indicate the Svalbard branch variation (Section A1) largely determine the interannual variation of mass and heat transport into the northern Barents Sea. In addition, local winds are likely to affect the inflow. Winters with intensified cold water formation in the northern Barents Sea could lead to increased outflow through the Franz Victoria Trough. The balanced mass flow in this trough might indicate this situation could be favourable for increased inflow.

Influence on northern Barents Sea hydrography: Case study 1995/1996.

The winter 1995/1996 was unusual in many respects. *Kwok et al.* (2005) showed the Barents Sea had especially high freshwater content and exceptionally high ice transport

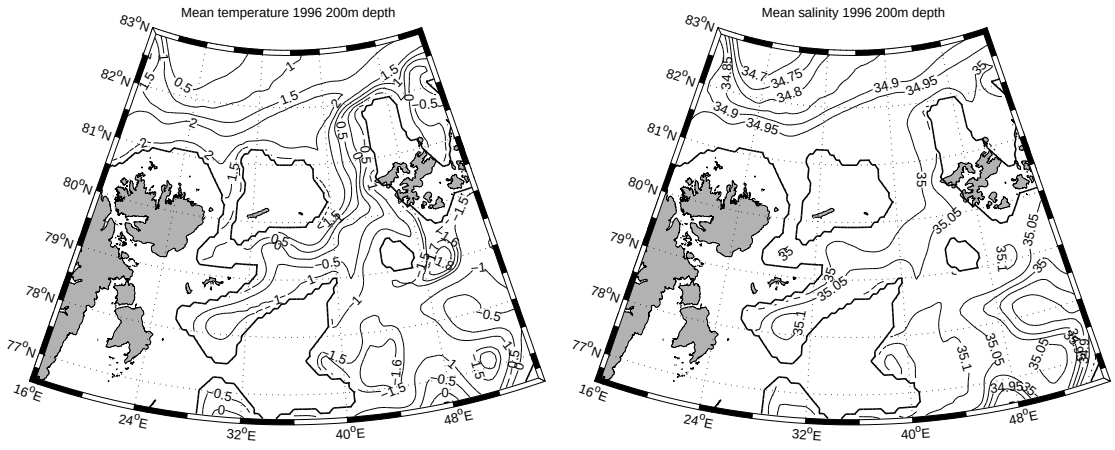

Figure 4.10: 1996 mean model temperature (left figure) and salinity (right figure) at 200 m depth.

from the Arctic Ocean to the Barents Sea this winter. Additionally, Figure 4.9 shows ROMS gave a significant drop in mass and heat transport of the Svalbard branch in 1995. The mentioned abnormalities of this winter could be related to a shift in the NAO index from a highly positive phase to a highly negative phase this winter. This change in NAO index means less westerly winds and reduced Norwegian Atlantic Current, hence colder air and less AW inflow to the Barents Sea.

Figure 4.10 shows the model temperature and salinity at 200 m depth in 1996. In comparison to the 12-year mean temperature and salinity at 200 m depth in Figure 3.7, it is clear ROMS give much higher salinities and slightly lower temperatures inside the northern Barents Sea at in 1996. Accordingly, this might indicate an increased dense water production in the northern Barents Sea this year. Figure 3.10 supports this conclusion as the model gives the bottom-intensified northward cold current on the eastern side of the Franz Victoria Trough increased velocity and extent in 1996. It is also seen the model gave an upper-level intensified southward current on the western side of the Franz Victoria Trough the same year.

Similar comparisons showed the model surface layer was much fresher and somewhat colder in 1996 than the 12-year mean (not shown), possibly caused by lower air temperature and less AW inflow in the upper layer (as discussed in Chapter 4.1.2 the model generally has AW inflow too high up in the water column, however not this year).

Sea ice transport through the Northern Barents Sea Opening

Kwok et al. (2005) investigated 10 years of satellite records 1994-2003 and found the direction of transport between the Arctic Ocean and the Barents Sea is controlled by the location of the mean atmospheric low in the Barents Sea. If the mean atmospheric low pressure is situated in the eastern Barents Sea and the winter Perennial Ice Zone is shifted southwards towards the northern Barents Sea, conditions are favourable for large inflows of multiyear ice into the northern Barents Sea. They find as many years with ice export from the Arctic to the Barents as opposite directed ice transport, adding up to 40 km^3 mean export from the Arctic through the NBSO with hugh variability ranging from -280 km^3 to 340 km^3. *Kwok et al.* (2005) also report a mean ice thickness of 2.5 m during a winter of net ice import to the Arctic, possibly an indication of thickness of first year ice in the northern Barents Sea.

Comparable water mass and flow structure in all openings of the Barents Sea

The typical water mass distribution and flow field of straits in ROMS have similarities to that seen in the Franz Victoria Trough in Figure 3.9. Warm water enters the Barents Sea on one side and cold water leaves the Barents Sea on the other side. The outflow typically has an intensified bottom boundary current with CBW, as observed in the BSX in 1991-1992 (*Gammelsrød et al.*, 2008) and modelled by ROMS in the Franz Victoria Trough. The geographical orientation of this simplified model of the Barents Sea straits is so that the cold flow is to the right of warm inflow, seen from inside the Barents Sea. This simplification of the water mass exchange between the Barents Sea and its surrounding oceans highlights the Barents Sea as a heat sink and modifier of AW.

Chapter 5

Summary and conclusions

By investigating a 9 km resolution simulation of ROMS and observations of hydrography and currents in the northern Barents Sea, new knowledge is provided about this relatively unexplored region.

First, validating ROMS results in the northern Barents Sea showed it generally gave too warm and saline water masses, at least in autumn when direct comparisons with observations were attainable. ROMS may also have too extensive water mass modification producing unrealistic amounts of cold, saline water. Apparently, ROMS is better at reproducing inflowing water masses than processes inside the northern Barents Sea, reflected in better agreement for Atlantic than Arctic and Surface Water.

Additionally, Figure 4.1 showed some lack of vertical fine structure in temperature and salinity. The model flow fields were highly barotropic and followed isobaths.

Connection between the northern and southern Barents Sea is limited by the saddle point between Hopen Trench and Olga Basin. The model flow and hydrography revealed ROMS allows AW from south to cross it. Additionally, observations may show modified AW from south in the northern Barents Sea (*Pfirman et al.*, 1994), and AW from north meeting AW from south in Figure 4.5 a).

The model flow field show some similarities the sparse amount of current measurements available (Figure 3.3; *Abrahamsen et al.* (2006)). The model results indicate ArW is formed in the northern Barents Sea rather than being transported into it from the Arctic Ocean. The inflow of AW through the two straits in the Northern Barents Sea Opening (NBSO) is an important heat source for the northern Barents Sea, even though not significant in the overall heat budget. Interestingly, the net heat transport of 7.6 TW into the Barents Sea was dominated by exchanges in Franz Victoria Trough, while the net mass transport of 0.33 Sv into the Barents Sea was mainly from inflow in the Kvitøya Strait.

Exchanges through the NBSO emphasizes the Barents Sea as a heat sink for the Arctic Ocean as the inflow is warm and the outflow is cold. This study also indicate water mass modifications in the northern Barents Sea is a source for Cold Halocline and Cold Bottom Water for the Arctic Ocean.

Model transports showed interannual variations of Svalbard branch mass and heat is responsible for nearly 50% of the interannual variation of mass, with a time lag of one year, and 37% of heat transport into the northern Barents Sea. Additionally, a close mass balance between outflow and inflow in the Franz Victoria Trough could indicate variations of cold water production inside the Barents Sea also affect exchanges in this trough.

The Persey Current, interpreted from observations of hydrography, does not compare with the model flow field.

References

Aagaard, K., L. Coachman, and E. Carmack (1981), On the halocline of the Arctic Ocean, *Deep-Sea Research*, *28*, 529–545.

Aagaard, K., A. Foldvik, T. Gammelsrød, and T. Vinje (1983), One-year records of current and bottom pressure in the strait between Nordaustlandet and Kvitøya, Svalbard, 1980-81, *Polar Research 1n.s.*, pp. 107–113.

Abrahamsen, E., S. Østerhus, and T. Gammelsrød (2006), Ice draft and current measurements from the north-western Barents Sea, 1993-96, *Polar Research*, *25*(1), 25–37.

Budgell, W. (2005), Numerical simulation of ice-ocean variability in the Barents Sea region. Towards dynamical downscaling, *Ocean Dynamics*, *55*, 370–387.

Gammelsrød, T., Ø. Leikvin, V. Lien, W. Budgell, H. Loeng, and W. Maslowski (2008), Mass and Heat Transports in the NE Barents Sea; Observations and Models, *Submitted*.

Gerdes, R., and U. Schauer (1997), Large-scale circulation and water mass distribution in the Arctic Ocean from model results and observations, *Journal of Geophysical Research*, *102*(C4), 8467–8483.

Gerdes, R., M. Kärcher, F. Kauker, and U. Schauer (2003), Causes and development of repeated Arctic Ocean warming events, *Geophysical Research Letters*, *30*(19), 1980 doi:101,029/2003GL018,080.

Harms, I. (1997), Water mass transformation in the Barents Sea - application of the Hamburg Shelf Ocean Model (HamSOM), *ICES Journal of Marine Science*, *54*, 351–365.

Harms, I., C. Schrum, and K. Hatten (2005), Numerical sensitivity studies on the variability of climate-relevant processes in the Barents Sea, *Journal of Geophysical Research*, *110, C06002, doi:10.1029/2004JC002559*.

Harris, C., A. Plueddemann, and G. Gawarkiewicz (1998), Water mass distribution and polar front structure in the western Barents Sea, *Journal of Geophysical Research*, *103*(C2), 2905–2918.

Helland-Hansen, B., and F. Nansen (1909), The Norwegian Sea, *Fisk. dir. Skr. Ser. Havunders.*, *2*(2), 1–360.

Ingvaldsen, R., H. Loeng, and L. Asplin (2002), Variability in the atlantic inflow to the barents sea based on a one-year time series from moored current meters, *Continental Shelf Research*, *22*(505-519).

Ingvaldsen, R., L. Asplin, and H. Loeng (2004), The seasonal cycle in the Atlantic transport to the Barents Sea during the years 1997-2001, *Continental Shelf Research*, *24*, 1015–1032.

Ivanov, V., I. Dmitrenko, E. Hansen, S. Kirillov, C. Mauritzen, I. Polyakov, H. Simmons, and L. Timokhov (2007), What happens with Atlantic Water entering the Arctic Ocean through the Fram Strait?, *Geophysical Research Abstracts*, *9*, 05,072.

Johannesen, O. M., and L. A. Foster (1978), A note on the topographically controlled oceanic polar front in the Barents Sea, *Journal of Geophysical Research*, *83*(C9), 4567–4571.

Kowalik, Z., and A. Y. Proshutinsky (1995), Topographic enhancement of tidal motion in the western Barents Sea, *Journal of Geophysical Research*, *100*(C2), 2613–2637.

Kwok, R., W. Maslowski, and S. Laxon (2005), On large outflows of Arctic sea ice into the Barents Sea, *Geophysical Research Letters*, *32(22):L22503, doi:10.1029/2005GL024485*.

Li, S., and T. A. McClimans (1998), The effects of winds over a barotropic retrograde slope current, *Continental Shelf Research*, *18*, 457–485.

Lien, V., W. Budgell, B. Ådlandsvik, and E. Svendsen (2006), Validating results from the model ROMS (Regional Ocean Modelling System), with respect to volume transports and heat fluxes in the Nordic Seas, *Fisken og havet*, *2*.

Loeng, H. (1991), Features of the physical oceanographic conditions in the Barents Sea, *Polar Research*, *10*, 5–18.

Loeng, H., V. Ozhigin, and B. Ådlandsvik (1997), Water fluxes through the Barents Sea, *ICES Journal of Marine Science*, *54*, 310–317.

Løyning, T. (2001), Hydrography in the north-western Barents Sea, July-August 1996, *Polar Research*, *20*(1), 1–12.

Maslowski, W., D. Marble, W. Walczowski, U. Schauer, J. Clement, and A. Semtner (2004), On climatological mass, heat and salt transports through the Barents Sea and Fram Strait from a pan-Arctic coupled ice-ocean model simulation, *Journal of Geophysical Research*, *109:C03032, doi:101029/2001JC0010139*.

Midttun, L. (1985), Formation of dense bottom water in the Barents Sea, *Deep Sea Res., Part A*, *32*, 1233–1241.

Nansen, F. (1906), Northern waters: Captein Roald Amundsen's oceanographic observations in the Arctic seas in 1901, *Skr. Nor. Vidensk. Selsk., Mat. Naturvidensk.*, *1*, 145 pp.

Pfirman, S., D. Bauch, and T. Gammelsrød (1994), The northern Barents Sea: water mass distribution and modification, in *The polar oceans and their role in shaping the global environment*, vol. 85, edited by O. Johannesen, pp. 77–94, Geophys. Monogr., Washington, D.C.: AGU.

Renfrew, I. A., G. W. K. Moore, P. S. Guest, and K. Bumke (2002), A comparison of surface layer and surface turbulent flux observations over the Labrador Sea with ECMWF analyses and NCEP reanalyses, *Journal of Physical Oceanography*, *32*, 283–400.

Rosenfeld, L. (1983), Code-1: Moored array and large-scale data report, *Code tech report no. 21*, WHOI.

Saloranta, T., and P. Haugan (2001), Interannual variability in the hydrography of Atlantic water northwest of Svalbard., *Journal of Geophysical Research*, *106*(C7), 13,931–13,943.

Schauer, U., R. Muench, B. Rudels, and L. Timokhov (1997), Impact of eastern Arctic shelf waters on the Nansen Basin intermediate layers, *Journal of Geophysical Research*, *102*(C2), 3371–3382.

Simonsen, K., and P. Haugan (1996), Heat budget of the Arctic Mediterranean and the sea surface heat flux parameterizations for the Nordic Seas, *Journal of Geophysical Research*, *101*(3), 6553–6576.

Skagseth, Ø., T. Furevik, R. Ingvaldsen, H. Loeng, K. Mork, K. Orvik, and V. Ozhigin (2008), Volume and heat transports to the Arctic Ocean via the Norwegian and Barents Seas, in *Arctic-Subarctic Ocean Fluxes: Defining the Role of the Northern Seas in Climate*, edited by R. Dickson, J. Meincke, and P. Rhines, Springer, in press.

Steele, M., J. Morison, and T. Curtin (1995), Halocline water formation in the Barents Sea, *Journal of Geophysical Research*, *100*(C1), 881–894.

Winsor, P., and G. Björk (2000), Polynya activity in the Arctic from 1958 to 1997, *Journal of Geophysical Research*, *105*(C4), 8789–8803.